report (in Japanese with English abstract). *Rinsho Shinkeigaku* 1990; **30**: 1252–1255.
15. Williams TL, Shaw PJ, Lowe J, Bate D, Ince PG. Parkinsonism in motor neuron disease: case report and literature review. *Acta Neuropathol* 1995; **89**: 275–283.
16. Su M, Wakabayashi K, Tanno Y, Inuzuka T, Takahashi H. An autopsy case of amyotrophic lateral sclerosis with concomitant Alzheimer's and incidental Lewy body disease (in Japanese with English abstract). *No to Shinkei* 1996; **48**: 931–936.
17. Gibb WR, Lees AJ. The relevance of the Lewy body to the pathogenesis of idiopathic Parkinson's disease. *J Neurol Neurosurg Psychiatry* 1988; **51**: 745–752.
18. Klos KJ, Ahlskog JE, Josephs KA *et al.* Alpha-synuclein pathology in the spinal cords of neurologically asymptomatic aged individuals. *Neurology* 2006; **66**: 1100–1102.
19. Tamura T, Yoshida M, Hashizume Y, Sobue G. Lewy body-related α-synucleino- pathy in the spinal cord of cases with incidental Lewy body disease. *Neuropathology* 2012; **32**: 13–22.
20. Oyanagi K, Wakabayashi K, Ohama E *et al.* Lewy bodies in the lower sacral parasympathetic neurons of a patient with Parkinson's disease. *Acta Neuropathol* 1990; **80**: 558–559.
21. Wakabayashi K, Takahashi H. The intermediolateral nucleus and Clarke's column in Parkinson's disease. *Acta Neuropathol* 1997; **94**: 287–289.
22. Geser F, Brandmeir NJ, Kwong LK *et al.* Evidence of multisystem disorder in whole-brain map of pathological TDP-43 in amyotrophic lateral sclerosis. *Arch Neurol* 2008; **65**: 636–641.
23. Nishihira Y, Tan CF, Toyoshima Y *et al.* Sporadic amyotrophic lateral sclerosis: widespread multisystem degeneration with TDP-43 pathology in a patient after long-term survival on a respirator. *Neuropathology* 2009; **29**: 689–696.
24. Majoor-Krakauer D, Ottman R, Johnson WG, Rowland LP. Familial aggregation of amyotrophic lateral sclerosis, dementia, and Parkinson's disease: evidence of shared genetic susceptibility. *Neurology* 1994; **44**: 1872–1877.
25. Gilbert RM, Fahn S, Mitsumoto H, Rowland LP. Parkinsonism and motor neuron diseases: twenty-seven patients with diverse overlap syndromes. *Mov Disord* 2010; **25**: 1868–1875.

CONTRASTING ECHOGENICITY IN FLEXOR DIGITORUM PROFUNDUS–FLEXOR CARPI ULNARIS: A DIAGNOSTIC ULTRASOUND PATTERN IN SPORADIC INCLUSION BODY MYOSITIS

YU-ICHI NOTO, MD,[1] KENSUKE SHIGA, MD,[1] YUKIKO TSUJI, MD,[1] MASAKI KONDO, MD,[1] TAKAHIKO TOKUDA, MD,[1] TOSHIKI MIZUNO, MD,[1] and MASANORI NAKAGAWA, MD[2]

[1]Department of Neurology, Graduate School of Medical Science, Kyoto Prefectural University of Medicine, 465 Kajii-cho, Kamigyo-ku, Kyoto 602-0841, Japan

[2]Graduate School of Medical Science, Kyoto Prefectural University of Medicine, Kyoto, Japan

Accepted 13 August 2013

ABSTRACT: *Introduction:* In this study we aimed to clarify whether muscle ultrasound (US) of the forearm can be used to differentiate between patients with sporadic inclusion body myositis (s-IBM) and those with s-IBM–mimicking diseases. *Methods:* We compared the echo intensity (EI) of the flexor digitorum profundus (FDP) muscle and the flexor carpi ulnaris (FCU) muscles in patients with s-IBM ($n = 6$), polymyositis/dermatomyositis (PM/DM; $n = 6$), and amyotrophic lateral sclerosis (ALS; $n = 6$). *Results:* We identified EI abnormalities in 100% of patients with s-IBM, 33% of those with PM/DM, and 33% of those with ALS. An "FDP–FCU echogenicity contrast," a US pattern involving a higher EI in the FDP than in the FCU, was observed in all patients with s-IBM, but in none of those with PM/DM or ALS. *Conclusions:* FDP–FCU echogenicity contrast in muscle US is a sensitive diagnostic indicator of s-IBM.

Muscle Nerve **49**: 745–748, 2014

Sporadic inclusion body myositis (s-IBM), one of the most common myopathies in older adults, is characterized by slowly progressive muscle weakness with a predilection for the quadriceps femoris and flexor digitorum profundus (FDP) muscles.[1,2] In needle electromyography (EMG), s-IBM can be confused with amyotrophic lateral sclerosis (ALS) because of the presence of so-called "neurogenic changes," such as high-amplitude and long-duration motor unit potentials. These findings may be indicative of motor units with hypertrophied myofibers in chronic myopathy.[3] Hokkoku *et al.* reported that examination of the FDP muscle in EMG can reduce the risk of making a misdiagnosis of ALS in patients with s-IBM.[4] Magnetic resonance imaging (MRI) of the forearm was also reported to be useful for diagnosis of s-IBM.[2] Selective involvement of the FDP has thus drawn attention in the clinical diagnosis of s-IBM.

Over the past few decades, high-frequency ultrasound (US) of muscles and peripheral nerves has emerged as a non-invasive and simple tool to assist in the diagnosis of neuromuscular disorders. Therefore, we employed US of the FDP to differentiate accurately between patients with s-IBM and those with other s-IBM–mimicking diseases.

METHODS

Subjects. Consecutive Japanese patients who presented with s-IBM (6 patients), polymyositis (PM; 2 patients), dermatomyositis (DM; 4 patients), or amyotrophic lateral sclerosis (ALS; 6 patients) at our hospital were enrolled. Informed consent was provided by all patients. The diagnosis of s-IBM or PM/DM was confirmed by muscle biopsy according to previously established criteria.[5,6] All ALS patients fulfilled the Awaji criteria for probable/definite ALS, or showed progressive muscle weakness compatible with ALS.

Ultrasound. US imaging for all patients was performed by the same physician (Y.N.) using a GE Logiq P5 system with a 10-MHz linear-array probe (GE Healthcare Japan, Tokyo, Japan). Each subject lay in the supine position with the right elbow bent. The transducer was placed at 5 cm distal to the right olecranon, as shown in Figure 1A. The FDP could be identified as a triangular compartment adjacent to the ulna. The ulnar nerve is a landmark for identification of the 3 muscles [the FDP, flexor digitorum superficialis (FDS), and flexor carpi ulnaris (FCU)], because the nerve is encircled by these muscles. This transducer placement provides a favorable cross-sectional view of the FDP and FCU muscles at the same depth to enable effective comparison of echo intensity (EI) between them. Machine settings for image acquisition were preset and kept constant for all images without adjusting the focal point, gain, or time-gain compensation settings.

Visual Assessment of Muscle Echo Intensity. The EI of the FDP muscle adjacent to the ulna was scored retrospectively by a single examiner (Y.N.), based on the Heckmatt rating scale, as follows:

Abbreviations: ALS, amyotrophic lateral sclerosis; CSA, cross-sectional area; DM, dermatomyositis; EI, echo intensity; EMG, electromyography; FCU, flexor carpi ulnaris; FDP, flexor digitorum profundus; FDS, flexor digitorum superficialis; MRI, magnetic resonance imaging; MUP, motor unit potential; PM, polymyositis; s-IBM, sporadic inclusion-body myositis; US, ultrasound

Key words: amyotrophic lateral sclerosis; diagnosis; inclusion body myositis; muscle; ultrasound

Correspondence to: Y. Noto; e-mail: y-noto@koto.kpu-m.ac.jp

Published online 27 August 2013 in Wiley Online Library (wileyonlinelibrary.com). DOI 10.1002/mus.24056

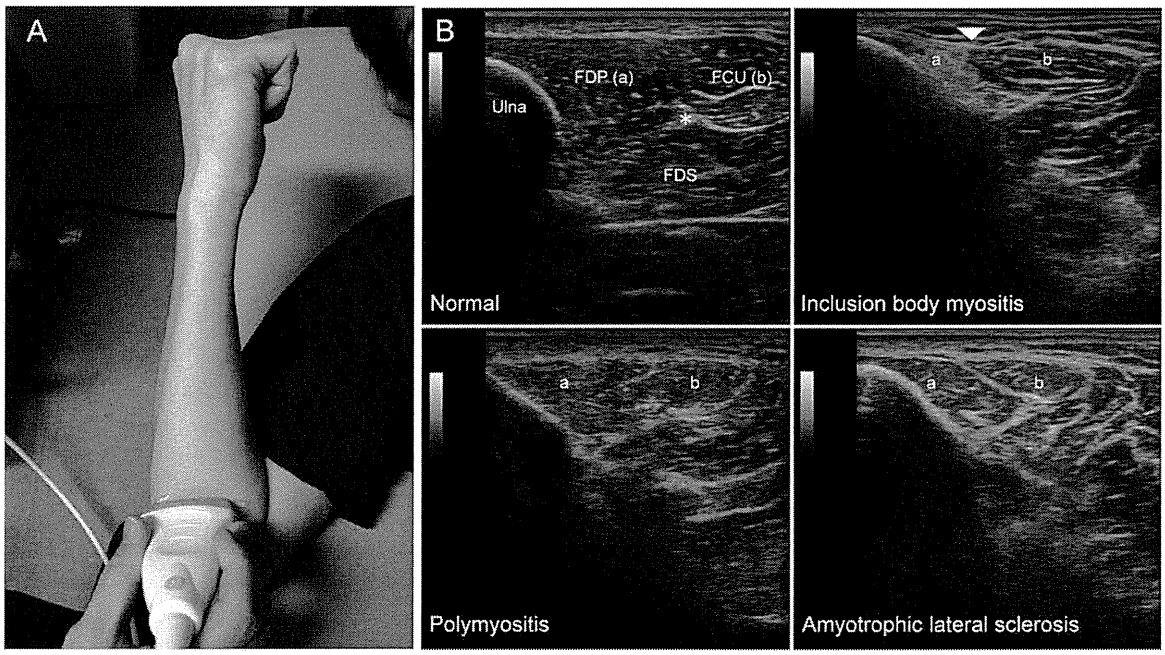

FIGURE 1. (A) Transducer position used to visualize the flexor digitorum profundus (FDP), flexor digitorum superficialis (FDS), and flexor carpi ulnaris (FCU) muscles simultaneously. The ulnar nerve (*) is encircled by the FDP, FDS, and FCU muscles. **(B)** Patterns of muscle ultrasound images in a normal subject, sporadic inclusion body myositis (s-IBM), polymyositis, and amyotrophic lateral sclerosis. Note the moderately high echo intensity of the FDP and normal echo intensity of the FCU in the s-IBM patient ("FDP–FCU echogenicity contrast") [arrow in **(B)**]. Slightly high echo intensities of the FDP and FCU muscles in PM and ALS patients.

1—normal; 2—slightly increased muscle EI with normal bone reflection; 3—moderately increased muscle EI with reduced bone reflection; and 4—severely increased muscle EI without bone reflection.[7] The Heckmatt grade of the FCU muscle was then scored by comparing it with that of the FDP muscle. A patient with increased "FDP–FCU echogenicity contrast" was indicated when the EI grade of the FDP muscle was $\geq$1 grade higher than that of the FCU muscle. The proportion of patients who had increased FDP–FCU echogenicity contrast was calculated in each disease group. In addition, FDP/FCU EI ratios (EI score of the FDP muscle divided by score of the FCU muscle) by Heckmatt rating scale scoring were also calculated.

Quantitative Assessment of Muscle Echo Intensity. Quantification of muscle EI using gray-scale analysis was performed to confirm the results obtained by visual assessment (i.e., Heckmatt rating scale score). This objective assessment was done with a standard histogram function available in Photoshop (Adobe Systems, Inc., San Jose, California), as reported previously.[8] The mean gray-scale values of FDP and FCU muscles were calculated, respectively, from the histogram, after encircling these muscles without surrounding fascia using the tracking software function. FDP/FCU EI ratios by gray-scale analysis were calculated.

Assessment of Muscle Atrophy. At the site described above, the muscle cross-sectional areas (CSAs) of the FDP and FCU were measured by continuous manual tracing of the muscle circumference, excluding the surrounding fascia. Measurement of the FDS muscle was omitted because a fraction of the circumference of the FDS muscle was often out of the cross-sectional image we obtained. FDP/FCU CSA ratios were calculated.

Statistical Analysis. All statistical analyses were performed using Stata software (StataCorp, College Station, Texas). Frequencies of all EI abnormalities and FDP–FCU echogenicity contrast detected by US were tested by the Fisher exact test. Multiple comparisons of Heckmatt rating scale scores, mean gray-scale values, FDP/FCU EI ratio of Heckmatt rating scale and gray-scale analysis, and FDP/FCU CSA ratio between the 3 groups were tested by analysis of variance and the Bonferroni procedure.

Standard Protocol Approvals. This study was approved by the local ethics committee of Kyoto Prefectural University of Medicine Graduate School of Medical Science.

RESULTS

Clinical Characteristics and Echo Intensity. Clinical profiles, Heckmatt rating scale scores for FDP and FCU, and detection rates of EI abnormalities and FDP–FCU echogenicity contrast are shown in Table 1. The mean Heckmatt rating scale score for the FDP and the FDP/FCU EI ratio by the Heckmatt rating scale were significantly higher in the s-IBM

Table 1. Demographics, clinical findings, and echo intensity abnormalities.

	s-IBM (n = 6)	PM/DM (n = 6)	ALS (n = 6)
Gender (M:W)	5:1	3:3	3:3
Age in years [mean (range)]	71.5 (68–79)	56.3 (39–72)	72.2 (62–79)
Disease duration in months [mean (range)]	56.7 (14–120)	49.3 (1–215)	29.8 (2–94)
Heckmatt rating scale of FDP [mean (range)]	2.7 (2–3)*,†	1.3 (1–2)	1.3 (1–2)
Heckmatt rating scale of FCU [mean (range)]	1.3 (1–2)	1.3 (1–2)	1.3 (1–2)
FDP/FCU Heckmatt rating scale ratio (mean)	2.2*,†	1.0	1.0
EI abnormality of any FDP and FCU muscle [n (%)]	6 (100)**,††	2 (33)	2 (33)
FDP–FCU echogenicity contrast [n (%)]	6 (100)**,††	0 (0)	0 (0)

FDP/FCU Heckmatt rating scale ratio is defined as EI score of the FDP muscle divided by EI score of the FCU muscle. EI abnormality is defined as Heckmatt rating scale score ≥2. FDP–FCU echogenicity contrast is defined as an echo intensity pattern of a higher intensity in FDP than in FCU muscle. s-IBM, sporadic inclusion body myositis; PM/DM, polymyositis/dermatomyositis; ALS, amyotrophic lateral sclerosis; EI, echo intensity; FDP, flexor digitorum profundus muscle; FCU, flexor carpi ulnaris muscle.

**$P < 0.05$ and **$P < 0.01$ vs. PM/DM.*

†$P < 0.05$ and ††$P < 0.01$ vs. ALS.

group than in the PM/DM or ALS groups. All s-IBM patients had EI abnormalities of the FDP muscle, whereas 2 of 6 PM/DM patients (33%) and 2 of 6 ALS patients (33%) had EI abnormalities. All EI abnormalities in the FDP muscles obtained from s-IBM arms showed a homogeneous high echoic pattern, whereas those obtained from the PM/DM and ALS arms showed a rather heterogeneous high echoic pattern, as shown in Figure 1B. On visual assessment, none of the s-IBM patients had an EI abnormality of the FCU, whereas 2 PM/DM patients and 2 ALS patients had increased EI in both the FCU and FDP muscles. In the PM/DM or ALS arms, no patients exhibited a higher EI in FDP than in FCU. Thus, the FDP/FCU echogenicity contrast pattern, indicating higher EI in FDP compared with the FCU muscle, was a characteristic finding in s-IBM patients (Fig. 1B). Quantitative analysis using gray-scale analysis also showed that the FDP/FCU EI ratio was significantly higher in the s-IBM group than in the PM/DM or ALS groups ($P < 0.01$ and $P < 0.01$, respectively). The mean FDP/FCU EI ratios of s-IBM, PM/DM, and ALS patients were 1.33, 0.88, and 1.02, respectively. No significant differences in any indices were found when comparing PM/DM and ALS groups.

Muscle Cross-Sectional Area. Muscle CSAs and FDP/FCU CSA ratios are shown in Table 2. No significant difference in CSA of the FDP muscle was found among the 3 groups, whereas CSAs of the FCU muscles in s-IBM were significantly larger than those in ALS patients. The FDP/FCU CSA ratio was significantly lower in the s-IBM group than in the PM/DM or ALS groups.

DISCUSSION

This study has revealed that patients with s-IBM show "FDP–FCU echogenicity contrast," in which the EI of the FDP muscle is higher than that of the FCU muscle. This recognizable EI pattern was not seen in any of the patients with PM/DM or those with ALS in this study. The results demonstrate that muscle US of the forearm is a non-invasive and easily accessible diagnostic tool for s-IBM.

A high EI in muscle US suggests increased fibrous tissue or fatty degeneration in interstitial components of the muscle, indicating chronic myopathy. A low EI reflects interstitial edema, which is often observed in the acute stage of inflammatory myopathy.[9,10] It remains to be elucidated whether s-IBM is caused by an inflammatory or a degenerative mechanism together with a secondary inflammatory process. In general, muscle biopsy of s-IBM patients reveals abundant chronic myopathic changes, such as marked variation in fiber size, endomysial fibrosis, and fatty degeneration. In this study, a visually homogeneous high echoic pattern

Table 2. Comparison of muscle cross-sectional area.

	s-IBM (n = 6)	PM/DM (n = 6)	ALS (n = 6)
CSA of FDP muscle (mm^2) [mean (range)]	80.5 (63.0–117.4)	165.9 (90.4–332.3)	106.3 (62.1–148.6)
CSA of FCU muscle (mm^2) [mean (range)]	131.8 (100.9–149.5)†	110.3 (73.9–135.6)	86.3 (49.4–129.4)
FDP/FCU CSA ratio (mean)	0.61*,†	1.47	1.28

FDP/FCU CSA ratio is defined as CSA of the FDP muscle divided by CSA of FCU muscle. s-IBM, sporadic inclusion body myositis; PM/DM, polymyositis/dermatomyositis; ALS, amyotrophic lateral sclerosis; CSA, cross-sectional area; FDP, flexor digitorum profundus muscle; FCU, flexor carpi ulnaris muscle.

**$P < 0.01$ vs. PM/DM.*

†$P < 0.05$ vs. ALS.

of the FDP muscle was found in s-IBM patients, whereas EI abnormality in muscle in ALS and PM/DM patients showed a rather heterogeneous pattern. Although we found that mean gray-scale values of the FDP in s-IBM were higher than those in PM/DM and ALS patients, it is unclear what determines the visual echoic pattern (i.e., homogeneous or heterogeneous). Further study related to the correlation between the visual ultrasound pattern and the muscle pathology of s-IBM is needed.

Sekul *et al.* reported that muscle MRI of the forearm demonstrated selective involvement of the FDP muscle in up to 95% of s-IBM patients.[2] Furthermore, they observed marbled brightness of the FCU and FDS muscles on T1-weighted MRI in 33% and 29% of patients, respectively, and concluded that the FDS muscle was spared even in the late stages of s-IBM. In addition, a quantitative motor unit potential (MUP) analysis revealed decreased amplitude, short duration, and reduced MUP size index in the FDP.[4] Both the MRI study and quantitative MUP indicated that selective involvement of the FDP can be a unique finding to identify patients with s-IBM. In this US study, the frequencies of a high EI of the FDP and FCU muscles were comparable to those of the MRI study (100% in FDP and 33% in FCU muscles), indicating that US image analysis is another promising technique to identify FDP muscle pathology. This study also revealed decreased FDP/FCU CSA ratios in s-IBM patients, indicating selective atrophy of the FDP. Among the various tests, muscle US is advantageous because it is not only less invasive than EMG or muscle biopsy, but it is also far less expensive than MRI. In addition, US assessment is readily available in any hospital and can be repeated easily at the bedside.

There are some limitations to this study. First, our findings were obtained from a small population of patients. Second, the patients with PM/DM in this study were younger than those with ALS. Muscle echo intensity increases with age due to replacement by fat or fibrous tissue.[8] This could have influenced the results of echo intensity in older patients to some extent. Finally, the US examinations in this study were done by a single examiner who was not blinded to the clinical diagnoses. A blinded design with a larger number of patients with inter- or intrarater reliability assessment will be needed to confirm the results of our study.

REFERENCES

1. Engel WK, Askanas V. Inclusion-body myositis: clinical, diagnostic, and pathologic aspects. Neurology 2006;66(suppl):S20–29.
2. Sekul EA, Chow C, Dalakas MC. Magnetic resonance imaging of the forearm as a diagnostic aid in patients with sporadic inclusion body myositis. Neurology 1997;48:863–886.
3. Eisen A, Berry K, Gibson G. Inclusion body myositis (IBM): myopathy or neuropathy? Neurology 1983;33:1109–1114.
4. Hokkoku K, Sonoo M, Higashihara M, Stålberg E, Shimizu T. Electromyographs of the flexor digitorum profundus muscle are useful for the diagnosis of inclusion body myositis. Muscle Nerve 2012;46: 181–186.
5. Needham M, Mastaglia FL. Inclusion body myositis: current pathogenetic concepts and diagnostic and therapeutic approaches. Lancet Neurol 2007;6:620–631.
6. Hoogendijk JE, Amato AA, Lecky BR, Choy EH, Lundberg IE, Rose MR, et al. 119th ENMC International Workshop: Trial design in adult idiopathic inflammatory myopathies, with the exception of inclusion body myositis, 10–12 October 2003, Naarden, The Netherlands. Neuromuscul Disord 2004;14:337–345.
7. Heckmatt JZ, Leeman S, Dubowitz V. Ultrasound imaging in the diagnosis of muscle disease. J Pediatr 1982;101:656–660.
8. Pillen S, Arts IM, Zwarts MJ. Muscle ultrasound in neuromuscular disorders. Muscle Nerve 2008;37:679–693.
9. Reimers CD, Fleckenstein JL, Witt TN, Muller-Felber W, Pongratz DE. Muscular ultrasound in idiopathic inflammatory myopathies of adults. J Neurol Sci 1993;116:82–92.
10. Arts IM, Schelhaas HJ, Verrijp KC, Zwarts MJ, Overeem S, van der Laak JA, et al. Intramuscular fibrous tissue determines muscle echo intensity in amyotrophic lateral sclerosis. Muscle Nerve 2012;45:449–450.

JNNP Online First, published on August 4, 2014 as 10.1136/jnnp-2014-308211

RESEARCH PAPER

Nerve ultrasound depicts peripheral nerve enlargement in patients with genetically distinct Charcot-Marie-Tooth disease

Yu-ichi Noto,[1] Kensuke Shiga,[2] Yukiko Tsuji,[1] Ikuko Mizuta,[1] Yujiro Higuchi,[3] Akihiro Hashiguchi,[3] Hiroshi Takashima,[3] Masanori Nakagawa,[4] Toshiki Mizuno[1]

[1]Department of Neurology, Graduate School of Medical Science, Kyoto Prefectural University of Medicine, Kyoto, Japan
[2]Department of Medical Education and Primary Care, Graduate School of Medicine, Kyoto Prefectural University of Medicine, Kyoto, Japan
[3]Department of Neurology and Geriatrics, Kagoshima University Graduate School of Medical and Dental Sciences, Kagoshima, Japan
[4]North Medical Center, Kyoto Prefectural University of Medicine, Kyoto, Japan

Correspondence to
Dr Yu-ichi Noto, Department of Neurology, Kyoto Prefectural University of Medicine Graduate School of Medical Science, 465 Kajii-cho, Kamigyo-ku, Kyoto 602-0841, Japan; y-noto@koto.kpu-m.ac.jp

Received 31 March 2014
Revised 6 July 2014
Accepted 13 July 2014

ABSTRACT

Objective To elucidate the ultrasound (US) features of peripheral nerves including nerve roots in patients with different types of Charcot-Marie-Tooth disease (CMT), and the association between US findings, clinical features and parameters of nerve conduction studies (NCS) in CMT1A.

Methods US of median, sural and great auricular nerves and the C6 nerve root was performed in patients with CMT1A (n=20), *MPZ*-associated CMT (n=3), *NEFL*-associated CMT (n=4), *EGR2*-associated CMT (n=1), *ARHGEF10*-associated CMT (n=1) and in controls (n=30). In patients with CMT1A, we analysed the correlations between US findings and the following parameters: age, CMT Neuropathy Score (CMTNS) and NCS indices of the median nerve.

Results Cross-sectional areas (CSAs) of all the nerves were significantly increased in patients with CMT1A compared with that in controls. In *MPZ*-associated CMT, increased CSAs were found in the median nerve at wrist and in the great auricular nerve, whereas it was not increased in patients with *NEFL*-associated CMT. In patients with CMT1A, there was a positive correlation between CMTNS and the CSAs in the median nerves or great auricular nerves. In median nerves in patients with CMT1A, we found a negative correlation between the nerve conduction velocity and the CSA.

Conclusions Nerve US may aid in differentiating among the subtypes of CMT in combination with NCS. In CMT1A, the median nerve CSA correlates with the disease severity and peripheral nerve function.

INTRODUCTION

Charcot-Marie-Tooth disease (CMT) is a clinically and genetically heterogeneous inherited neuropathy, characterised by distal muscle atrophy, weakness and sensory loss with reduced tendon reflexes. Nerve conduction studies (NCS) differentiate CMT into the demyelinating type (median nerve motor conduction velocity (MCV) <38 m/s) and axonal type (median nerve MCV >38 m/s).[1] Autosomal dominant (AD) demyelinating (CMT1), AD axonal (CMT2), autosomal recessive (AR; CMT4) and X linked (CMTX) forms of CMT exist. The main pathology of CMT4 is demyelinating. CMTX type 1 (CMT1X) is the second most common form of CMT. Most males with CMT1X have intermediately slow MCV between 30 and 45 m/s, and the pathology of CMT1X is axonal loss and some segmental demyelination.[2] Over the last decade, there have been rapid advances in identifying genetic abnormalities in patients with CMT. More than 45 different CMT-causing genes have been described.[3] Furthermore, Hattori *et al*[4] reported that patients with *MPZ*, *PMP2* and *Cx32* mutations present both demyelinating and axonal types.

High-resolution ultrasound (US) has been increasingly used for the non-invasive assessment of peripheral nerve diseases.[5 6] US features of some CMT subtypes have been reported.[7 8] Schreiber *et al*[9] reported direct comparisons of nerve US findings between CMT subtypes and the correlation between nerve US indices and NCS parameters. However, detailed studies, including those on US assessment of nerve roots and clarification of the correlation between US findings and the disease severity, remain limited.

The purpose of this study was to describe US features of peripheral nerves including C6 nerve root in different types of CMT, and analyse the correlation between US findings and clinical/neurophysiological parameters.

METHODS

The study was conducted at Kyoto Prefectural University of Medicine Hospital between January and November 2012. Informed consent was provided by each participant, and the study protocol was conducted in accordance with the Declaration of Helsinki.

Subjects

We examined 35 consecutive patients (21 males and 14 females; age range 10–80 years; mean±SD 46.7±19 years) with hereditary motor and sensory neuropathy, 4 of whom were blood relatives to at least one other patient of the study group. In all patients, the diagnosis was based on the results of NCS and a family history of the disease.

Thirty sex-matched and age-matched controls (19 males and 11 females; age range 24–84 years; mean±SD 42.7±16 years) were recruited from the staff of Kyoto Prefectural University of Medicine and their families, who were free of any neuromuscular symptoms (eg, numbness and tingling or weakness of limbs), diabetes mellitus and alcoholism.

Genetic testing

First, we investigated whether patients with the demyelinating type of CMT have PMP22 duplication or deletion by fluorescence in situ hybridisation. For patients with the demyelinating type of CMT who

To cite: Noto Y, Shiga K, Tsuji Y, *et al*. *J Neurol Neurosurg Psychiatry* Published Online First: [*please include* Day Month Year] doi:10.1136/jnnp-2014-308211

had no *PMP22* rearrangement or patients with the axonal type of CMT, genomic DNA was extracted from their peripheral blood leucocytes, and then 30 disease-causing genes related to CMT were screened for using the custom MyGeneChip CustomSeq Resequencing Array (Affymetrix, Inc, Santa Clara, California, USA), which was designed to screen for CMT and related diseases, such as ataxia with oculomotor apraxia types 1 and 2, spinocerebellar ataxia with axonal neuropathy and distal hereditary motor neuropathy.[10] We designed 363 primer sets to include the entire coding regions and flanking sequences of the 30 genes (box 1). When a novel mutation was detected, we performed familial segregation analysis to elucidate the pathogenicity of the mutation if possible.

Ultrasound

All US examinations were performed by the same examiner (Y-iN) trained in neuromuscular US, using a GE Logic P5 System (GE Healthcare Japan, Tokyo, Japan) with a 12 MHz linear-array probe. The cross-sectional areas (CSAs) of the following nerves and nerve roots were measured: median nerve, sural nerve, great auricular nerves and C6 nerve root. Additionally, the diameter of the C6 root was measured. The median and the sural nerves were selected for evaluation because those nerves have been frequently evaluated in preceding studies in patients with CMT. The greater auricular nerve was examined because of the unique travelling course in the neck surface and its easy accessibility. The examiner (Y-iN) was not blinded to the diagnosis or clinical or electrophysiological findings. All participants were placed in a supine position when their median nerves and cervical nerve roots were examined, and in a prone position when their sural nerves were examined. The median nerve was imaged at the wrist crease, in the middle of the forearm, and in the middle of the upper arm. The sural nerve was imaged at 10 cm proximal to the lateral malleolus. We used the saphenous vein as a landmark when we identified the sural nerve beside the vein. The great auricular nerve was imaged at the midpoint between the top of the sternum and mandibular angle. We could identify the nerve in front of the sternocleidomastoid muscle (figure 1A). The CSAs were calculated by manual tracking of the nerve circumference including the hyperechoic rim. The diameter of the root was measured between the outer surfaces of the hyperechoic rims. The measured site of the C6 nerve root was about 1 cm distal to the transverse process after identifying the C6 vertebra using a previously reported procedure (figure 1B).[11]

Box 1 Genes analysed in the screening

PMP22 (peripheral myelin protein 22)
MPZ (myelin protein zero)
EGR2 (early growth response 2)
NEFL (neurofilament light chain polypeptide)
ARHGEF10 (rho guanine-nucleotide exchange factor 10)
GJB1 (gap junction protein beta 1)
PRX (periaxin)
LITAF (lipopolysaccharide-induced TNF-α factor)
GDAP1 (ganglioside-induced differentiation-associated protein 1)
MTMR2 (myotubularin-related protein 2)
SH3TC2 (SH3 domain and tetratricopeptide repeats 2)
SBF2 (SET-binding factor 2)
NDRG1 (N-myc downstream regulated 1)
MFN2 (mitofusin 2)
RAB7 (Ras-related GTPase 7)
GARS (glycyl-tRNA synthetase)
HSPB1 (heat shock protein 1)
HSPB8 (heat shock protein 8)
LMNA (lamin A/C)
DNM2 (dynamin 2)
YARS (tyrosyl-ARS)
AARS (alanyl-ARS)
KARS (lysyl-ARS)
APTX (aprataxin)
SETX (senataxin)
TDP1 (tyrosyl-DNA phosphodiesterase 1)
SOX10 (SRY-BOX 10)
DHH (desert hedgehog)
GAN1 (gigaxonin 1)
KCC3 (K-Cl cotransporter family 3)

Nerve conduction studies

Using standard techniques (Neuropack EMG system (Nihon Kohden, Tokyo, Japan)), conventional NCS was performed. The skin temperature was maintained above 32°C. The distal motor latency (DML), compound muscle action potential (CMAP) amplitude and MCV were recorded from the median nerve. The MCV was assessed in the wrist to elbow. The sensory nerve action potential (SNAP) amplitude, SNAP duration and sensory conduction velocity (SCV) were recorded from median and sural nerves. Antidromic median and sural nerve SNAPs were recorded from digit II and behind the lateral malleolus, respectively. We analysed the corresponding nerves in unilateral side using US and NCS.

Clinical assessment

Patients with CMT underwent clinical and neurophysiological assessment based on the CMT Neuropathy Score (CMTNS).[12] The CMTNS is composed of nine items: sensory symptoms, motor symptoms of legs and arms, pin sensibility, vibration, strength of legs and arms, ulnar CMAP amplitude and ulnar SNAP amplitude. The CMTNS ranges from 0 (no deficit) to 36 (maximal deficit).

Statistics

In the analysis of NCS parameters, if no CMAP and SNAP responses were elicited, they were excluded from analysis except for the amplitude data (CMAP and SNAP amplitudes in no response were regarded as 0.001 mV and 0.001 μV, respectively). Fisher's exact test was used to analyse the gender ratio between patients with CMT and controls. To compare CMTNS between the different CMT subgroups, and the US parameters (CSA and diameter) among the different CMT subgroups and controls, a Bonferroni-corrected Mann-Whitney U test was applied. The correlation between the US findings (CSA and diameter) and clinical parameters (age, height, weight, body mass index and CMTNS) or the electrophysiological parameters (DML, MCV, SCV, CMAP amplitude and SNAP amplitude) in controls and patients with CMT1A was tested with Pearson correlation coefficients. In all comparisons, a p value of less than 0.05 was considered significant. All statistical analyses were performed using STATA software (Stata Corp, Texas, USA).

RESULTS

Clinical data and CMTNS

On the basis of the genetic testing results, 20 patients were classified with *PMP 22* duplication-associated CMT (CMT1A), 3 with *MPZ*-associated CMT (2 CMT1B and 1 CMT2J), 4 with

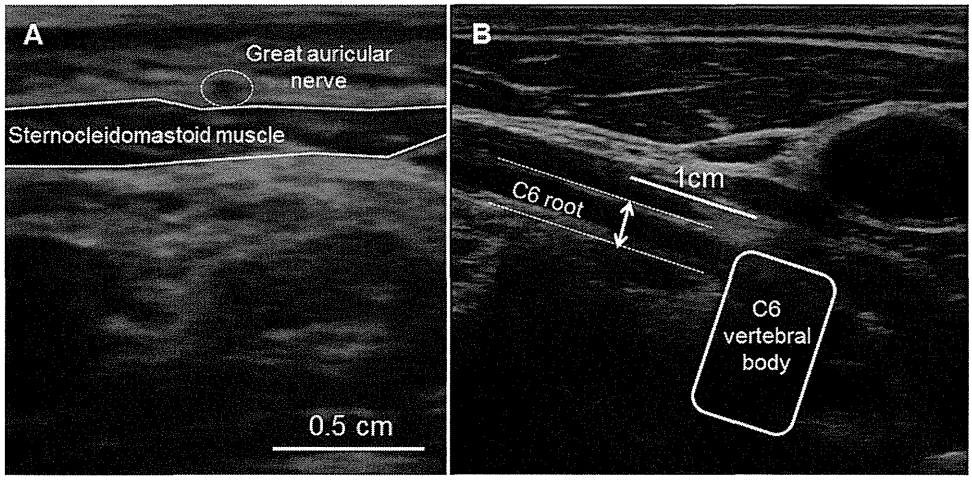

Figure 1 The ultrasound images of the great auricular nerve (A) and the measured site in the C6 nerve root (B). The dotted circle indicates the cross-sectional image of the great auricular nerve (A). The distances between the outer surfaces of the hyperechoic rims (between arrowheads) were measured as the nerve root diameter (B).

NEFL-associated CMT (2 CMT1F and 2 CMT2E), 1 with *EGR2*-associated CMT and 1 with *ARHGEF10*-associated CMT. The patient with CMT2J presented hearing loss and autonomic dysfunction such as Adie's pupils and dysuria, in addition to the distal dominant muscle weakness. All of the patients with *NEFL*-associated CMT showed distal dominant muscle weakness. The patient with *EGR2*-associated CMT was reported by us recently.[13] The patient with *ARHGEF10*-associated CMT presented muscle weakness in lower extremities with a slight decrease in vibratory sensation. Direct sequencing of the *ARHGEF10* gene in the patient with *ARHGEF10*-associated CMT revealed a heterozygous single nucleotide substitution, c.2435T>C, which might be a novel mutation. We could confirm the same mutation in the proband's brother with similar symptoms and electrophysiological findings, although gene analysis of other asymptomatic family members was not possible. No pathogenic mutation was identified in three patients with demyelinating type CMT and three with axonal type CMT.

Demographic data, the electrophysiological neuropathy type, CMTNS and gene mutation of each CMT subtype are shown in table 1. No significant difference in CMTNS was demonstrated among the CMT subtypes. In groups with *MPZ* or *NEFL* mutation, demyelinating and axonal types were mixed.

US findings

US findings in each CMT group and the control group are presented in table 2 and figure 2. The CSAs in patients with CMT1A were larger than those in controls irrespective of examination sites (figure 2). Although all mean CSAs and the C6 root diameter in patients with *MPZ* mutation tended to be larger than in controls, significant differences existed in the median nerve CSA at wrist and in the great auricular nerve CSA. There were no significant differences between all CSAs in patients with *NEFL* mutation and controls, whereas median nerve CSAs at three sites in patients with CMT1A were larger than in patients with *NEFL* mutation including the demyelinating type. In a patient with *EGR2* mutation, CSAs of proximal sites tended to be large, and the C6 root CSA in a patient with *EGR2* mutation was larger than the mean CSA value+2 SDs in controls. Although we could not identify the C6 root and great auricular nerve in a patient with *ARHGEF10* mutation, CSAs of the median nerve and sural nerve in the patient were slightly larger than the mean CSAs of controls.

Nerve conduction studies

Results of parameters of the NCS on the median and the sural nerves are listed in table 3. In patients with CMT1A, motor and

Table 1 Biometric data, electrophysiological neuropathy types, CMT Neuropathy Score and gene mutations

	PMP22 duplication (n=20)	*MPZ* mutation (n=3)	*EFL* mutation (n=4)	*EGR2* mutation (n=1)	*ARHGEF10* mutation (n=1)	Controls (n=30)
Age, mean (range)	47.6 (21–78)	39.7 (10–69)	47.3 (27–68)	49	67	42.7 (24–84)
Gender (M/F)	10/10	2/1	2/2	0/1	1/0	19/11
Height (cm), mean (SD)	161.9 (10.0)	152.7 (16.1)	168.4 (5.1)	160.0 (NA)	173.5 (NA)	162.8 (11.5)
Weight (kg), mean (SD)	58.2 (11.1)	55.6 (17.5)	63.5 (22.2)	56.0 (NA)	76.0 (NA)	58.4 (10.8)
Body mass index, mean(SD)	22.1 (3.3)	23.4 (2.5)	22.3 (7.6)	23.8 (NA)	25.2 (NA)	21.9 (2.2)
Demyelinating type/axonal type	20/0	2/1	2/2	1/0	0/1	NA
CMT Neuropathy Score, mean (range)	14.0 (7–28)	12.0 (10–14)	15.5 (9–25)	7.0	7.0	NA
Gene mutations	PMP22 duplication	CMT1B: Tyr68Cys (n=2); CMT2J: Thr124Met	CMT1F: Pro8Leu (n=2) CMT2E: Glu396Lys; Tyr389Cys	Thr387Asn	Thr109Ile	NA

CMT, Charcot-Marie-Tooth disease; F, female; M, male; NA, not applicable.

Table 2 Ultrasound findings in patients with Charcot-Marie-Tooth disease and controls

	PMP22 duplication (n=20)		*MPZ* mutation (n=3)		*NEFL* mutation (n=4)		*EGR2* mutation (n=1)		*ARHGEF10* mutation (n=1)		Controls (n=30)	
	Mean (SD)	(n)	Mean (SD)	(n)	Mean (SD)	(n)	Mean (SD)	(n)	Mean (SD)	(n)	Mean (SD)	(n)
Cross sectional area (mm^2)												
Median nerve (wrist)	23.5 (4.0)	(20)	21.0 (4.5)	(3)	12.0 (3.0)	(4)	20.5	(1)	22.8	(1)	14.1 (2.6)	(30)
Median nerve (forearm)	22.1 (9.2)	(20)	17.5 (8.9)	(3)	8.5 (3.1)	(4)	12.2	(1)	18.3	(1)	8.7 (1.3)	(30)
Median nerve (upper arm)	42.4 (11.8)	(20)	28.9 (12.3)	(3)	18.2 (4.4)	(4)	34.5	(1)	36.6	(1)	16.5 (2.7)	(30)
C6 root	29.8 (10.7)	(12)	17.0	(1)	17.1	(1)	42.2	(1)	NA	(0)	13.0 (3.1)	(22)
Great auricular nerve	3.9 (1.6)	(19)	5.2 (3.8)	(2)	2.0	(1)	3.5	(1)	NA	(0)	1.7 (0.6)	(25)
Sural nerve	11.0 (4.8)	(20)	7.5 (2.5)	(3)	6.0 (2.5)	(4)	6.7	(1)	14.3	(1)	5.8 (1.5)	(29)
Diameter (mm)												
C6 root	5.3 (1.1)	(13)	4.4	(1)	4.1	(1)	5.5	(1)	NA	(0)	3.6 (0.5)	(25)

NA, not applicable.

sensory conduction velocities reduced with decreased CMAP and SNAP amplitude. In patients with *MPZ* mutation, the patients with CMT1B had a very slow MCV, whereas the patient with CMT2J showed a nearly normal MCV. In patients with *NEFL*-mutations, the difference between CMT1F and 2E was similar to that between CMT1B and 2J. The patient with *EGR2*-associated CMT (CMT1D) showed a demyelinating pattern. The MCV and SCV were moderately slowed in the patient with *ARHGEF10* mutation.

Correlation between US findings and clinical/electrophysiological parameters in patients with CMT1A

We analysed the correlation between US findings (nerve CSAs and C6 diameter) and clinical data (CMTNS, age, height, weight and body mass index)/electrophysiological parameters in patients with CMT1A. The CMTNS in patients with CMT1A was positively correlated with the CSA of the great auricular nerve and that of the median nerve at the upper arm (figure 3A, B). Moreover, an inverse association was noted between the C6 root CSAs and age

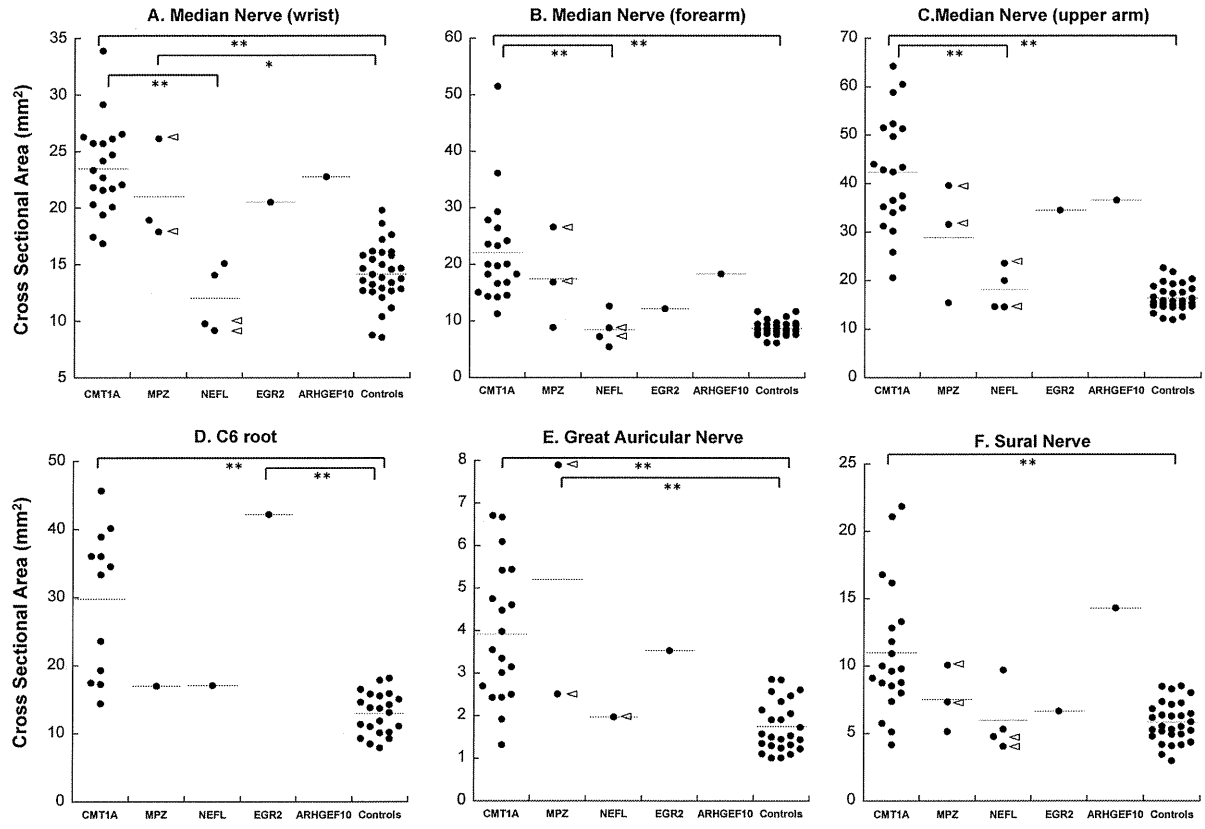

Figure 2 Ultrasound data on the median nerve, C6 root, great auricular nerve and sural nerve in patients with Charcot-Marie-Tooth disease (CMT) and controls. Horizontal bars indicate means. *p<0.05; **p<0.01. Arrowheads indicate demyelinating type in patients with *MPZ*-associated and *NEFL*-associated CMT. Cross-sectional areas of the C6 root and great auricular nerve in patients with *ARHGEF10*-associated CMT were not recorded because of technical difficulty in ultrasound examination.

Table 3 Nerve conduction study results

	Median nerve (motor)			Median nerve (sensory)		Sural nerve	
	DML (ms)	Amplitude (mV)	MCV (m/s)	Amplitude (μV)	SCV (m/s)	Amplitude (μV)	SCV (m/s)
PMP22 duplication (n=20)	10.2	3.8	21.8	1.3	20.9	0.6	22.9
MPZ mutation (n=3)							
CMT1B (n=2)	6.9	4	14.6	0.0	NA	0.0	NA
CMT2J (n=1)	3.7	11.3	46.4	9.7	49.4	6	51.9
NEFL mutation (n=4)							
CMT1F (n=2)	8.0	2.4	24.2	0.0	NA	0.0	NA
CMT2E (n=2)	5.7	9.8	50.4	6.8	43.5	1.3	54.9
EGR2 mutation (n=1)	6	4.7	23.2	2.1	26.8	NE	NA
ARHGEF10 mutation (n=1)	4.7	5.6	41.7	14.7	40.2	6.5	48.8

Data are given as means.
CMT, Charcot-Marie-Tooth disease; DML, distal motor latency; MCV, motor conduction velocity; NE, not evoked; NA, not applicable; SCV, sensory conduction velocity.

(figure 3C). Although statistically significant differences were not demonstrated, age tends to correlate inversely with CSAs of the median nerve at the fore arm, that at upper arm, the sural nerve and the great auricular nerve, whereas a positive relationship between age and CSAs of median nerve at the wrist was observed ($p=0.23$). All clinical data except for the CMTNS and age showed no correlation with CSAs and the C6 diameter.

In the analysis between US findings of the median nerve and electrophysiological parameters, there was a significant negative correlation between the CSA at the forearm and MCV of the median nerve (between the wrist and elbow; $p<0.05$; figure 4A). Likewise the CSA at the upper arm of the median nerve was negatively correlated with the MCV of the median nerve (between the wrist and elbow; $p<0.01$; figure 4B). No correlation was observed between the CSA and CMAP amplitude/SNAP amplitude of the median nerve. Analysis of the correlation between US and electrophysiological findings of the sural nerve was not performed because SNAPs were not evoked in 18 of the 20 patients with CMT1A.

DISCUSSION

In this study, we confirmed that patients with CMT1A showed a uniform enlargement of nerves, including the nerve root, based on US imaging. Although small in number, we showed increased CSA in median nerves in individuals with *MPZ* mutations (CMT1B and 2J), *EGR2* mutations (CMT1D) and *ARHGEF10* mutations. In patients with *NEFL* mutations (CMT1F and 2E), however, the CSAs in the examined nerves are comparable to those in normal controls. This is the first report regarding the US findings in patients with CMT2J, 1F, 2E, 1D and *ARHGEF10*-associated CMT. The limitation of this study included a small number of patients with rare mutations. Therefore, these findings should be confirmed in a larger cohort in the future. Furthermore, we revealed not only the presence of a correlation between the CSAs and electrophysiological parameters, but also a correlation between the CSAs and clinical parameters (CMTNS) in patients with CMT1A.

In agreement with previous reports, we found markedly increased CSAs in all nerves and nerve roots in patients with CMT1A.[6–9 14] The ranges of CSAs in great auricular and sural nerves of patients with CMT1A and controls overlapped to some extent (figure 2). Measuring CSAs in the median nerve and nerve root may facilitate a clear distinction among CMT1A, *NEFL*-associated CMT and a healthy state. Pazzaglia *et al*[15] reported that the sural nerve CSA was not increased in the majority of patients with CMT1A (70%). In our study, however, the sural nerve CSA in patients with CMT1A was significantly larger than that in controls. One of the factors influencing the difference between our results and the aforementioned study might be that CSAs were calculated by tracking the nerve circumference including the hyperechoic rim in that study. We measured CSAs by tracking the outline of the hyperechoic rim in consideration of the possibility that the nerve stroma including the epineurium proliferates in some subtypes of CMT. Robaglia-Schlupp *et al*[16] reported that PMP22 overexpression enhanced collagen synthesis by fibroblasts, and noted the possibility that structures other than Schwann cells were affected in CMT1A.

In this study, three patients with *MPZ* mutations were included. Two of them were diagnosed with CMT1B. The remaining patient was diagnosed with CMT2J. There have been no reports including US findings in patients with CMT2J. CSAs in all nerves of the patient with CMT2J were the smallest in the three patients with *MPZ*-associated CMT, and these, excluding the median nerve (wrist) of the patient with CMT2J, were nearly the same as the mean values of the control group. Median nerve CSAs of the other two patients with demyelinating-type *MPZ*-associated CMT (CMT1B) tended to be larger than in controls (figure 2). These findings are consistent with a previous study on CMT1B.[8]

This is the first report on nerve US findings including patients with *NEFL*-associated CMT. Four patients with *NEFL*-associated CMT were examined in this study, comprising two with CMT1F and two with CMT2E. Although two of the four patients had demyelinating-type CMT, they did not show the enlargement of peripheral nerves. The *NEFL* gene encodes the neurofilament light chain polypeptide (NEFL), which is one of the most abundant cytoskeletal components of neurons, and plays a pivotal role in the assembly and maintenance of the axonal cytoskeleton. Fabrizi *et al*[17] noted that the main pathological finding in patients with *NEFL*-associated CMT was axonopathy with marked structural alterations in the cytoskeleton and significant secondary demyelination. It appears that nerve conduction velocity slowing in *NEFL*-associated CMT is associated with mutations affecting the NEFL protein head domain.[18] From these findings, patients with demyelinating type CMT may not always present increased CSAs of nerves, although previous studies have reported that patients with other demyelinating type CMT generally showed increased CSAs of nerves.[9 19]

The patient with *EGR2*-associated CMT in this study presented with a mild, demyelinating, adult-onset form.[13] The *EGR2* gene encodes early growth response-2 protein (EGR2), which plays a role in peripheral nerve myelin development and maintenance, and

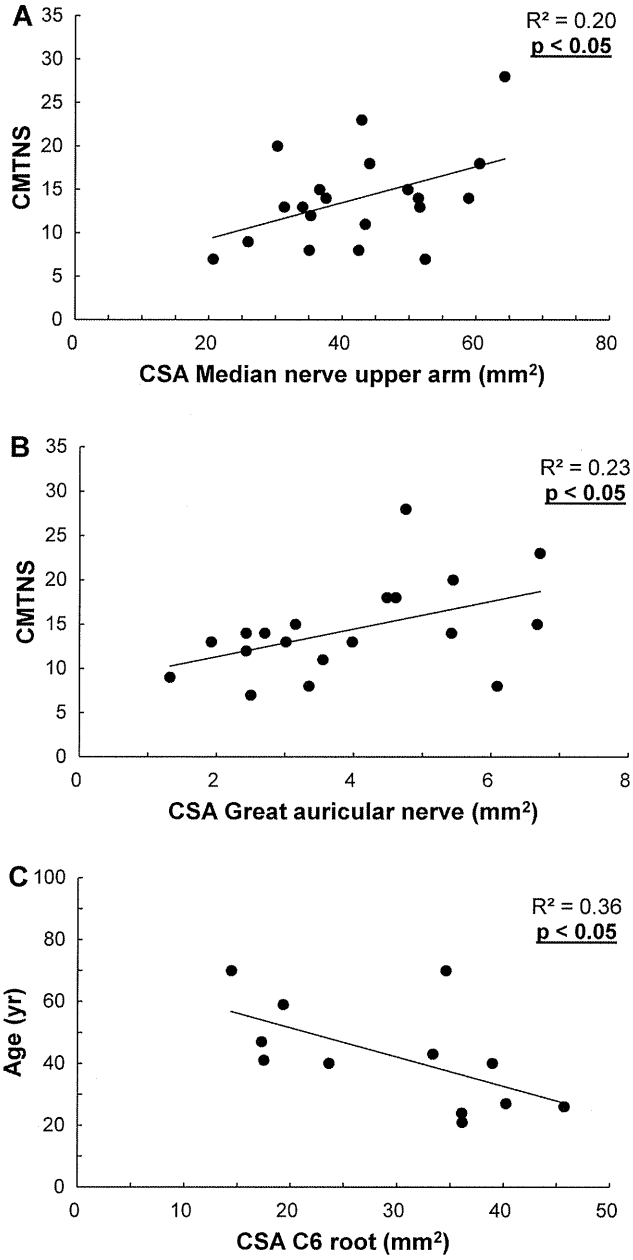

Figure 3 Scatterplot of the clinical parameters and ultrasound findings in patients with CMT1A. The CMTNS was positively correlated with the CSA of the great auricular nerve and that of the median nerve at the upper arm (A and B). An inverse correlation between the C6 root CSAs and age was observed (C). CMTNS, CMT neuropathy score; CSA, cross-sectional area; CMT, Charcot-Marie-Tooth disease.

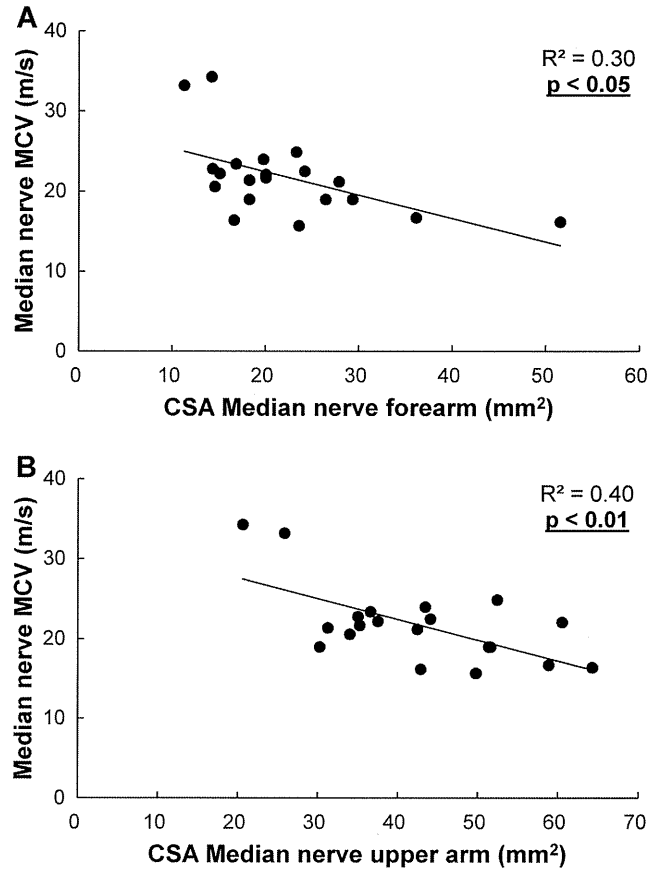

Figure 4 Scatterplot of the electrophysiological parameters and ultrasound findings in patients with CMT1A. A negative correlation between the CSA at the forearm and MCV of the median nerve (between the wrist and elbow) was found (A). Likewise the CSA at the upper arm of the median nerve was negatively correlated with the MCV of the median nerve (between the wrist and elbow) (B). CMT, Charcot-Marie-Tooth disease; CSA, cross-sectional area; MCV, motor conduction velocity.

activates the transcription of several myelin-associated genes, such as *PMP22* and *MPZ*. Although we could include only one patient with *EGR2*-associated CMT, CSAs in all nerves tended to be larger than in controls. We also included the patient with CMT who had a potent novel mutation in the *ARHGEF10* gene, as aforementioned. The phenotype of the patient was classified as the axonal type by neurophysiological testing, but the MCV was moderately slowed (median nerve MCV 41.7 m/s), as well as in previous studies.[20 21] Verhoeven *et al* demonstrated the possibility that ARHGEF10 protein is associated with the developmental myelination of peripheral nerves using a mouse model. CSAs in all nerves were increased in the present patient, although CSAs of the C6 root and great auricular nerve were not recorded because of technical difficulties.

Regarding the US findings of the patients with CMT1A, Pazzaglia *et al*[15] demonstrated an inverse correlation between sural nerve CSAs and the age in patients with CMT1A. In this study, no such correlation was observed in patients with CMT1A. As aforementioned, the difference in the method of measuring CSAs could influence the results. Instead, a significant negative correlation between C6 root CSAs and the age was noted. However, there are some reports that the biometric data of patients with CMT showed no significant correlation with CSAs.[7 9] Thus, the results of correlation analysis between CSAs and biometric data have varied among reports. The reason for this remains unclear, and so further studies involving larger series of cases are needed.

This study first showed the correlation between the disease severity (CMTNS) and CSAs in patients with CMT1A. Patients with a larger CSA in the median or great auricular nerve may show more marked impairment. It is extrapolated from these results that the degree of the disease severity might be determined by the extent of the pathological change, such as onion bulbs which are the results of repetitive demyelination–remyelination and the proliferation of the nerve stroma. On the other hand, it seems that the positive relationship between CMTNS and CSAs contradicts the inverse relationship between age and CSAs in this study (figure 3), because CMTNS generally increases with age in patients with CMT. Future studies will be

required to elucidate whether age or disease severity has more influence on the nerve enlargement in CMT1A. Along with the report by Pazzaglia *et al*,[15] the negative correlation between age and CSAs in most of the nerves might be specific to CMT1A, and indicates that decreased CSAs reflect axonal loss. Conversely, only CSA in median nerve at wrist correlated with age positively in patients with CMT1A of this study, although it was not statistically significant. CSA at wrist might be affected by factors except for CMT1A including carpal tunnel syndrome (CTS), etc. In patients with CTS, median nerve CSAs at wrist are generally increased.[22]

Several studies have reported on the relationships between US findings and NCS parameters in CMT and other neuropathies.[7 9 23–25] Consistent with a previous study by Schreiber *et al*, we identified a significant negative correlation between the CSAs of median nerve and the MCVs in the corresponding segment. The decreased MCVs in patients with CMT1A reflect the functional aspect for the histopathological alteration of myelination, progression of which might have paralleled the enlargement of nerves, that is, increased CSAs.

There are some limitations to our study. First, US examinations were performed by only one unblinded examiner. However, Cartwright *et al*[26 27] reported that the diagnostic accuracy of neuromuscular US in unblinded studies was similar to that in blinded studies, and that intra-rater and inter-rater reliability of nerve and muscle US were sufficiently high. This argument may mitigate the unblinded design in this study to some extent; however, blinded assessment by multiple examiners is desirable in future studies on nerve US. Second, the small number of some CMT types is also a limitation of our study. Therefore, the findings of CSAs obtained from a single or a few patients should be carefully interpreted. Further study of a large population is needed, especially in *MPZ*-associated and *NEFL*-associated CMT in which demyelinating and axonal types are mixed. Third, the US feature of CMT1A has been already revealed by some studies.[5–7 9 14] However, describing the US finding of that was needed for shedding light on the extent of nerve enlargement in other rare CMT subtypes. In addition, nerve CSAs correlated with the clinical severity in CMT1A can provide a new insight into the evolving field of nerve US. Finally, our CSA measuring method including the hyperechoic rim is different from the method in most previous studies of nerve US with tracking inside the rim. Therefore, US findings in our study should be compared with other studies of nerve US with caution. However, our method might make it possible to assess the actual pathology of CMT because structures other than Schwann cells could proliferate in CMT1A.[16]

In conclusion, we have demonstrated US findings at diverse anatomical sites of patients with CMT subtypes. We confirmed the uniform enlargement of peripheral nerves in patients with CMT1A. We also found that patients with demyelinating-type CMT, such as CMT1F (*NEFL*-associated CMT), do not always exhibit nerve enlargement. Nerve US in addition to conventional NCS could facilitate targeted gene analysis in clinical situations, and may advance the understanding of peripheral nerve pathology in patients with CMT.

Contributions Y-iN was involved in design of the study, analysis of the data and drafting of the manuscript. KS was involved in design of the study, acquisition and interpretation of data and revision of the manuscript. YT was involved in interpretation of the data. IM was involved in acquisition and analysis of the data. YH, AH and HT were involved in acquisition and analysis of the data and drafting of the manuscript. MN was involved in design of the study and revision of the manuscript.

Funding The work was partly funded by the Intramural Research Grant for Neurological and Psychiatric Disorders of NCNP, Applying Health and Technology of Ministry of Health, Welfare and Labour, Japan and Grants-in-Aid from the Research Committee of Charcot-Marie-Tooth Disease, the Ministry of Health, Labour and Welfare of Japan.

Competing interests None.

Ethics approval The local ethics committee of Kyoto Prefectural University of Medicine.

Provenance and peer review Not commissioned; externally peer reviewed.

REFERENCES

1 Harding AE, Thomas PK. The clinical features of hereditary motor and sensory neuropathy types I and II. *Brain* 1980;103:259–80.
2 Shy ME, Siskind C, Swan ER, *et al*. CMT1X phenotypes represent loss of GJB1 gene function. *Neurology* 2007;68:849–55.
3 Murphy SM, Laura M, Fawcett K, *et al*. Charcot-Marie-Tooth disease: frequency of genetic subtypes and guidelines for genetic testing. *J Neurol Neurosurg Psychiatry* 2012;83:706–10.
4 Hattori N, Yamamoto M, Yoshihara T, *et al*. Demyelinating and axonal features of Charcot-Marie-Tooth disease with mutations of myelin-related proteins (PMP22, MPZ and Cx32): a clinicopathological study of 205 Japanese patients. *Brain* 2003;126:134–51.
5 Heinemeyer O, Reimers CD. Ultrasound of radial, ulnar, median, and sciatic nerves in healthy subjects and patients with hereditary motor and sensory neuropathies. *Ultrasound Med Biol* 1999;25:481–5.
6 Zaidman CM, Al-Lozi M, Pestronk A. Peripheral nerve size in normals and patients with polyneuropathy: an ultrasound study. *Muscle Nerve* 2009;40:960–6.
7 Martinoli C, Schenone A, Bianchi S, *et al*. Sonography of the median nerve in Charcot-Marie-Tooth disease. *AJR Am J Roentgenol* 2002;178:1553–6.
8 Cartwright MS, Brown ME, Eulitt P, *et al*. Diagnostic nerve ultrasound in Charcot-Marie-Tooth disease type 1B. *Muscle Nerve* 2009;40:98–102.
9 Schreiber S, Oldag A, Kornblum C, *et al*. Sonography of the median nerve in CMT1A, CMT2A, CMTX, and HNPP. *Muscle Nerve* 2013;47:385–95.
10 Zhao Z, Hashiguchi A, Hu J, *et al*. Alanyl-tRNA synthetase mutation in a family with dominant distal hereditary motor neuropathy. *Neurology* 2012;78:1644–9.
11 Matsuoka N, Kohriyama T, Ochi K, *et al*. Detection of cervical nerve root hypertrophy by ultrasonography in chronic inflammatory demyelinating polyradiculoneuropathy. *J Neurol Sci* 2004;219:15–21.
12 Shy ME, Blake J, Krajewski K, *et al*. Reliability and validity of the CMT neuropathy score as a measure of disability. *Neurology* 2005;64:1209–14.
13 Shiga K, Noto Y, Mizuta I, *et al*. A novel EGR2 mutation within a family with a mild demyelinating form of Charcot-Marie-Tooth disease. *J Peripher Nerv Syst* 2012;17:206–9.
14 Sugimoto T, Ochi K, Hosomi N, *et al*. Ultrasonographic nerve enlargement of the median and ulnar nerves and the cervical nerve roots in patients with demyelinating Charcot-Marie-Tooth disease: distinction from patients with chronic inflammatory demyelinating polyneuropathy. *J Neurol* 2013;260:2580–7.
15 Pazzaglia C, Minciotti I, Coraci D, *et al*. Ultrasound assessment of sural nerve in Charcot-Marie-Tooth 1A neuropathy. *Clin Neurophysiol* 2013;124:1695–9.
16 Robaglia-Schlupp A, Pizant J, Norreel JC, *et al*. PMP22 overexpression causes dysmyelination in mice. *Brain* 2002;125:2213–21.
17 Fabrizi GM, Cavallaro T, Angiari C, *et al*. Charcot-Marie-Tooth disease type 2E, a disorder of the cytoskeleton. *Brain* 2007;130:394–403.
18 Miltenberger-Miltenyi G, Janecke AR, Wanschitz JV, *et al*. Clinical and electrophysiological features in Charcot-Marie-Tooth disease with mutations in the NEFL gene. *Arch Neurol* 2007;64:966–70.
19 Zaidman CM, Harms MB, Pestronk A. Ultrasound of inherited vs. acquired demyelinating polyneuropathies. *J Neurol* 2013;260:3115–21.
20 De Jonghe P, Timmerman V, Nelis E, *et al*. A novel type of hereditary motor and sensory neuropathy characterized by a mild phenotype. *Arch Neurol* 1999;56:1283–8.
21 Verhoeven K, De Jonghe P, Van de Putte T, *et al*. Slowed conduction and thin myelination of peripheral nerves associated with mutant rho Guanine-nucleotide exchange factor 10. *Am J Hum Genet* 2003;73:926–32.
22 Nakamichi K, Tachibana S. Ultrasonographic measurement of median nerve cross-sectional area in idiopathic carpal tunnel syndrome: diagnostic accuracy. *Muscle Nerve* 2002;26:798–803.
23 Scheidl E, Bohm J, Simo M, *et al*. Ultrasonography of MADSAM neuropathy: focal nerve enlargements at sites of existing and resolved conduction blocks. *Neuromuscul Disord* 2012;22:627–31.
24 Watanabe T, Ito H, Sekine A, *et al*. Sonographic evaluation of the peripheral nerve in diabetic patients: the relationship between nerve conduction studies, echo intensity, and cross-sectional area. *J Ultrasound Med* 2010;29:697–708.
25 Tsukamoto H, Granata G, Coraci D, *et al*. Ultrasound and neurophysiological correlation in common fibular nerve conduction block at fibular head. *Clin Neurophysiol* 2014;125:1491–5.
26 Cartwright MS, Hobson-Webb LD, Boon AJ, *et al*. Evidence-based guideline: neuromuscular ultrasound for the diagnosis of carpal tunnel syndrome. *Muscle Nerve* 2012;46:287–93.
27 Cartwright MS, Demar S, Griffin LP, *et al*. Validity and reliability of nerve and muscle ultrasound. *Muscle Nerve* 2013;47:515–21.

doi:10.1111/ncn3.152

ORIGINAL ARTICLE

Pharmacokinetics of levodopa/benserazide versus levodopa/carbidopa in healthy subjects and patients with Parkinson's disease

Hirotaka Iwaki,[1] Noriko Nishikawa,[1] Masahiro Nagai,[1] Tomoaki Tsujii,[1] Hayato Yabe,[1] Madoka Kubo,[1] Ichiro Ieiri[2] and Masahiro Nomoto[1]

[1]Department of Neurology and Clinical Pharmacology, Ehime University Graduate School of Medicine, Tohon, Ehime, and [2]Department of Clinical Pharmacokinetics, Graduate School of Pharmaceutical Science, Kyushu University, Maidashi Higashiku, Fukuoka, Japan

Key words
benserazide, carbidopa, levodopa, Parkinson's disease, pharmacokinetics.

Accepted for publication 30 October 2014.

Correspondence
Masahiro Nagai
Department of Neurology and Clinical Pharmacology, Ehime University Graduate School of Medicine, Tohon Ehime 791-0295, Japan.
Email: mnagai@m.ehime-u.ac.jp

Abstract

Background: There are two formulations of levodopa in Japan and a few other countries, levodopa/benserazide 100/25 mg and levodopa/carbidopa 100/10 mg, which have been generally regarded as interchangeable in Parkinson's disease treatment.

Aim: We investigated the pharmacokinetics of levodopa in the two kinds of levodopa/decarboxylase inhibitor (benserazide or carbidopa) formulations to study their equivalence.

Methods: Population pharmacokinetic analysis was carried out using levodopa data from the healthy subject study and, additionally, for 70 plasma concentration data points from Parkinson's disease patients receiving either levodopa/decarboxylase inhibitor combination in clinical practice.

Results: In healthy subjects, the mean ± standard deviation plasma levodopa maximum observed plasma concentration and area under the plasma concentration time curve from time 0 to 3 h (512 ± 139 *vs* 392 ± 49 μmol•h/L, $P < 0.05$) were significantly higher after levodopa/benserazide compared with levodopa/carbidopa. Levodopa time to maximum observed plasma concentration and plasma elimination half-life were not significantly different when comparing the respective formations. Levodopa pharmacokinetic parameters were the same between the Parkinson's disease patients and healthy subjects, except for levodopa apparent clearance, which was approximately two-thirds lower in Parkinson's disease patients compared with healthy subjects for both levodopa/decarboxylase inhibitor combinations, which might result in higher levodopa area under the curve in patients with Parkinson's disease than in healthy volunteers.

Conclusion: Levodopa pharmacokinetics differ after administration of levodopa/benserazide and levodopa/carbidopa. This information cold be useful for adjustment of medication in Parkinson's disease patients, especially with motor complications.

Introduction

Parkinson's disease (PD) is a neurodegenerative disease characterized by progressive loss of dopamine neurons in the substantia nigra and striatum. The shortage of dopaminergic input results in motor symptoms, such as rigidity, akinesia, tremor and postural instability, which is termed PD.

The cardinal treatment for patients with PD is oral administration of levodopa with peripheral decarboxylase inhibitor (DCI).[1] There are two DCI in clinical use: benserazide and carbidopa. In combination with levodopa, they are generally regarded as equally effective.[2,3] The clinical effectiveness was measured, however, in limited clinical settings, and there is little known about their pharmacokinetic differences.

Levodopa treatment is sufficient for patients with early-stage disease, but is associated with motor complications in late-stage disease, when substantial degeneration of nigrostriatal dopaminergic neurons has occurred. As the presynaptic handling and storage of levodopa-derived dopamine is reduced, the strength of dopaminergic stimulation becomes strictly dependent on the plasma levodopa concentration associated with motor complications, such as "wearing off"

and dyskinesia.[4] Drug dose adjustment should be considered carefully to maintain the serum levodopa concentration in the therapeutic window for patients with late-stage PD.

The aim of the present study was to determine whether there is any difference between the two levodopa/DCI combinations in terms of plasma levodopa concentrations. This information will be of clinical utility in achieving more effective treatment for PD.

Methods

Both studies were reviewed and approved by the institutional review board of Ehime University Hospital, and followed the ethical principles of the Declaration of Helsinki. Informed consent was obtained from each participant.

Pharmacokinetic study in healthy volunteers. A single-dose, cross-over study was undertaken in 10 young (age range 23–41 years) male volunteers to determine the pharmacokinetics of levodopa and DCI after the administration of a fixed-dose combination tablet of levodopa/benserazide or levodopa/carbidopa. All participants received a single tablet of levodopa 100 mg plus benserazide 25 mg and, after a 14-day washout period, a single tablet of levodopa 100 mg plus carbidopa 10 mg. The drugs were administered after overnight fasting, and the participants remained fasting throughout blood sampling.

Venous blood samples (5-mL aliquots into ethylenediaminetetraacetic acid-2Na tubes) were taken immediately before drug administration and every 30 min until 3 h. Blood samples were centrifuged for 10 min at 1000 *g*, and plasma was collected and stored at –80°C until measurement. Plasma concentrations of levodopa were measured using high-performance liquid chromatography (HPLC) with electrochemical detection. Plasma aliquots (100 μL) were mixed with 500 μL of ice-cold 0.2 mol/L perchloric acid containing 0.1 mmol/L ethylenediaminetetraacetic acid and 5 μL of 15 pg/mL 3,4-dihydroxybenzamine. Samples were centrifuged at 20 000 *g* for 15 min at 4°C (Himac CF 16RX; Hitachi, Tokyo, Japan). The supernatant was filtered through a 0.45-μm membrane filter (Chromatodisc 4A; GL Science, Tokyo, Japan), and a 10-μL aliquot of filtered solution was injected into the HPLC system with an electrochemical detector. The HPLC system included a delivery pump, a degasser and an electrochemical detector (HTEC-500; Eicom, Kyoto, Japan) with a Gilson 234 autoinjector (Eicom). Analytical separation was carried out on a reverse-phase column (C18 phase; 150 × 2.1 mm; EICOMPAK SSC-5-ODS, Eicom) at 30°C. The mobile phase consisted of 12% (v/v) methanol containing 0.1 mol/L phosphate buffer (pH 2.7) and 232 mg/L sodium octyl sulfate. The flow rate was maintained at 0.25 mL/min. Plasma concentrations of benserazide and carbidopa were measured with the same preparation with the mobile phase consisting of 12% of (v/v) methanol containing 0.1 mol/L phosphate buffer (pH 2.7) and 100 mg/L sodium octyl sulfate.

Pharmacokinetic parameters such as maximum observed plasma concentration (C_{max}), time to C_{max} (T_{max}) and plasma elimination half-life ($t_{1/2}$), and area under the plasma concentration-time curve from time 0 to 3 h ($AUC_{0-3\ h}$) were determined for levodopa and benserazide or carbidopa in each participant (Phoenix WinNonLin version 6.1, Certara, L.P., St. Louis, MO, USA). C_{max} and T_{max} were obtained directly from experimental data, and $t_{1/2}$ was calculated from the slope of the plasma concentration–time curve during the elimination phase. AUC was calculated using the linear trapezoidal rule. Data are presented as mean values ± SD. Paired data were compared using the Wilcoxon signed-rank test, and *P*-values <0.05 were considered significant.

Population pharmacokinetic study. A population pharmacokinetic study of levodopa was carried out among PD patients after the administration of a levodopa/DCI for comparison with results in healthy participants. The study population included PD patients attending our outpatient clinic who had been taking the previously described formulations of levodopa/benserazide or levodopa/carbidopa at therapeutic doses. Any patient receiving a catechol-O-methyl transferase inhibitor (COMT-I) was excluded, as such drugs potentially affect the metabolism of levodopa. A total of 47 blood samples were collected from 32 patients (14 men and 18 women; age 69 ± 12 years) taking levodopa/benserazide, and 23 blood samples were collected from 16 patients (8 men and 8 women; age 64 ± 10 years) taking levodopa/carbidopa. All blood samples were taken in the morning in a non-fasted state, and the duration between drug administration and taking of blood samples was recorded, as well as the drug dose they were receiving. Blood sampling, plasma collection and storage, and determination of levodopa concentrations were as described previously for healthy subjects.

Non-linear, mixed-effect modeling was used for pharmacokinetics analysis using NONMEM software (version 7.2.2; ICON Development Solutions, Ellicott City, MD, USA). Different structural models were tested and pharmacokinetic parameters, such as the absorption rate constant (K_a), apparent total body clearance (CL/F) and apparent volume of distribution (Vd/F), were estimated for each combination (levodopa/benserazide and levodopa/carbidopa) in each group (healthy subjects and patients) using first-order conditional estimation method with interaction (FOCE-INTER).

Results

Pharmacokinetic study in healthy volunteers. Plasma levodopa concentration versus time curves after administration of levodopa/benserazide 100/25 mg and levodopa/carbidopa 100/10 mg are shown in Figure 1a. Mean levodopa C_{max} was significantly higher after the administration of levodopa/benserazide 100/25 mg than after levodopa/carbidopa 100/10 mg (8.37 ± 3.19 *vs* 4.95 ± 1.65 μmol/L, $P < 0.001$). Mean T_{max} (33.0 ± 9.5 *vs* 51.0 ± 31.8 min) and $t_{1/2}$ (72.0 ± 15.3 *vs* 82.7 ± 24.0 min) for levodopa were not significantly different when comparing levodopa/benserazide 100/25 mg and levodopa/carbidopa 100/10 mg, respectively. Mean levodopa $AUC_{0-3\ h}$ was significantly higher after the administration of levodopa/benserazide 100/25 mg than after levodopa/carbidopa 100/

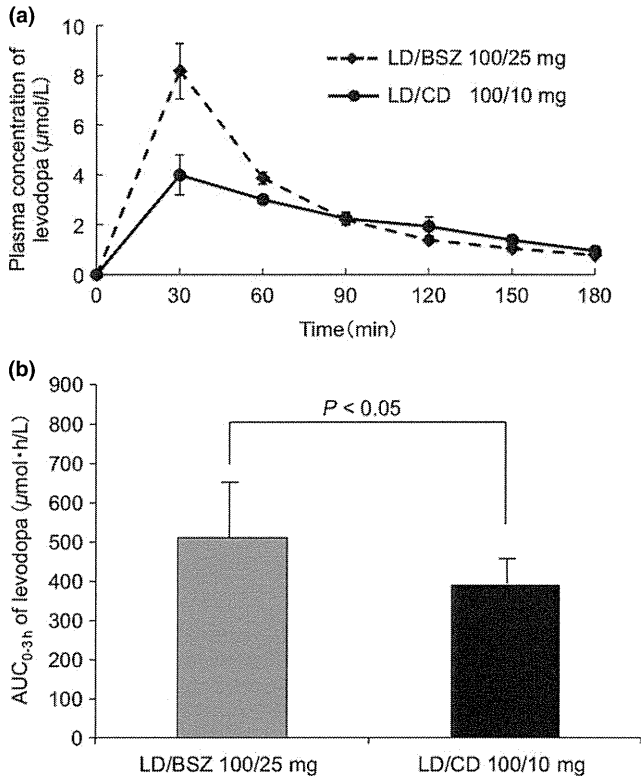

Figure 1 Levodopa pharmacokinetics in healthy subjects after administration of levodopa/benserazide 100/25 mg (LD/BSZ) or levodopa/carbidopa 100/10 mg (LD/CD). (a) Plasma concentration versus time curve. (b) Area under the plasma concentration–time curve from time 0 to 3 h ($AUC_{0-3\ h}$). Values are mean ± SD.

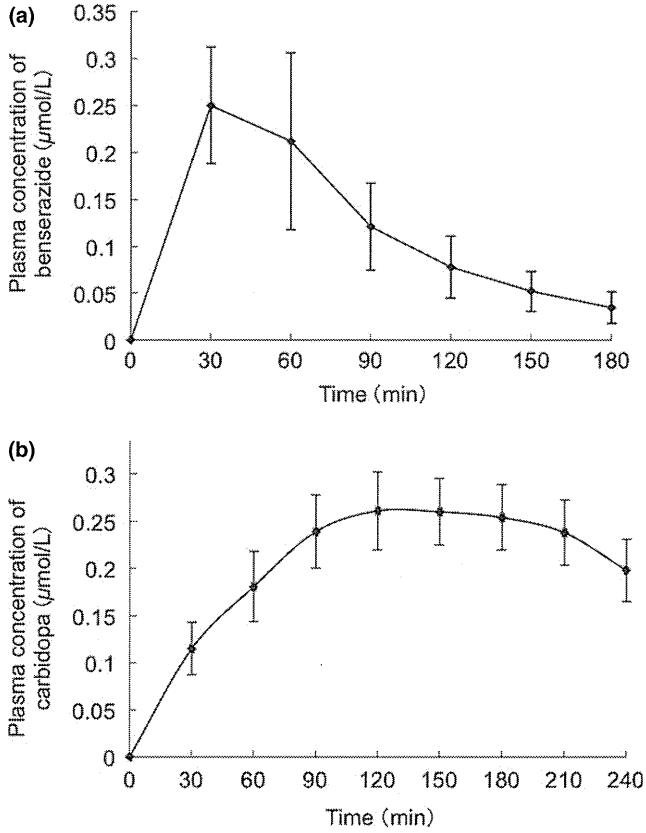

Figure 2 Plasma concentrations of (a) benserazide and (b) carbidopa in healthy subjects after administration of levodopa/benserazide 100/25 mg or levodopa/carbidopa 100/10 mg, respectively. Values are mean ± SD.

10 mg (511 ± 139 *vs* 391 ± 49 μmol•h/L, $P < 0.05$; Fig. 1b).

Plasma concentration versus time curves for benserazide and carbidopa after administration of levodopa/benserazide 100/25 mg and levodopa/carbidopa 100/10 mg are shown in Figure 2a,b, respectively. The following pharmacokinetic parameters were found for benserazide after the administration of levodopa/benserazide 100/25 mg: mean C_{max} 0.287 ± 0.174 μmol/L, T_{max} 36.0 ± 12.6 min and $t_{1/2}$ 48.6 ± 12.1 min. The following pharmacokinetic parameters were found for carbidopa after the administration of levodopa/carbidopa 100/10 mg: mean C_{max} 0.292 ± 0.078 μmol/L and T_{max} 147 ± 39 min. The $t_{1/2}$ was not determined, because four of the 10 participants did not reach the elimination phase within the observation period (up to 4 h after the administration).

Population pharmacokinetics. Figure 3a,b shows the plasma levodopa concentration for individual patients at various time-points after administration of levodopa in combination with benserazide or carbidopa, respectively. Concentrations of levodopa were generally higher after administration of levodopa/benserazide compared with levodopa/carbidopa. Population pharmacokinetics of levodopa were best described by a one-compartment model.

Estimated pharmacokinetic parameters are summarized in Table 1. As all the blood samples were taken at least 1 h after medication, it was not possible to estimate the absorption rate constant (K_a). K_a was therefore fixed at 10/min. Levodopa CL/F was lower after the administration of levodopa/benserazide as compared with levodopa/carbidopa in both healthy participants (0.734 *vs* 0.889 L/min) and patients (0.493 *vs* 0.555 L/min), although the differences were small. CL/F was consistently lower in patients as compared with healthy participants. Levodopa Vd/F was smaller after the administration of levodopa/benserazide as compared with levodopa/carbidopa in both healthy participants (44.7 *vs* 80.0 L) and patients (55.0 *vs* 81.4 L).

Discussion

Our cross-over study in healthy subjects showed that the pharmacokinetics of levodopa were different after oral administration of levodopa/benserazide 100/25 mg and levodopa/carbidopa 100/10 mg, even though these formulations are generally regarded as providing identical levodopa exposure in practice in Japan and a few other countries. In the non-compartmental analysis among the healthy subjects, mean C_{max} of levodopa was 1.7-fold higher and

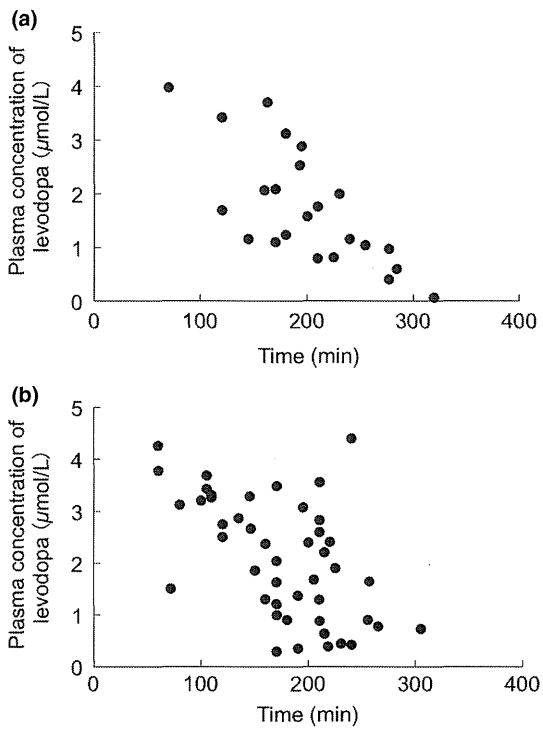

Figure 3 Plasma levodopa concentrations for individual patients with Parkinson's disease after administration of (a) levodopa/benserazide or (b) levodopa/carbidopa. Plasma levodopa concentration equivalent to a 100 mg dose plotted versus the time from dosing to sampling.

$AUC_{0-3\ h}$ was 1.3-fold larger with levodopa/benserazide as compared with levodopa/carbidopa. As levodopa dosing was the same (100 mg) for both formulations, it is assumed that benserazide 25 mg has a more significant inhibitory effect towards AADC than carbidopa 10 mg. Levodopa $t_{1/2}$ in the levodopa/benserazide group was shorter, but not significantly, compared with the levodopa/carbidopa group. It is interesting to note the different pharmacokinetics of the two DCI; that is, benserazide showed a rapid increase and rapid decrease in its plasma concentration, whereas carbidopa showed a slow increase and slow decrease in its plasma concentration. One possible explanation for the similarity of levodopa $t_{1/2}$ with both levodopa/DCI combinations might be that the DCI pivotally provided their inhibitory effects of AADC in the gut where extensive presystemic levodopa metabolism takes place, and systemic DCI only have limited efficacy for maintaining plasma levodopa levels.[5] Another levodopa metabolizer, COMT, could play an important role in this phenomenon. COMT is regarded as a predominant metabolizer when the AADC pathway is blocked.[6] Thus, it might compensate for the effect of systemic DCI against levodopa metabolism. We did not examine downstream products of levodopa metabolism in the present study, and this needs to be further investigated to clarify the mechanistic differences between levodopa $t_{1/2}$ and DCI pharmacokinetics. Additionally, we cannot exclude the possibility of ordering effect because of the non-randomized cross-over design of the study; however, we consider the effect to be negligible for the following three reasons. First, the 14-day washout period was long enough to eliminate the possibility of any carry-over effect. Second, the washout period was not so long that the conditions of the study participants and the surrounding co-factors were likely to have changed significantly during the period. Finally, drug concentration is an objective marker, so it was not affected by participants' subjective reactions.

The present population pharmacokinetic study showed that levodopa CL/F and Vd/F were lower after administration of levodopa/benserazide compared with levodopa/carbidopa in both healthy subjects and patients. The difference in levodopa CL/F and Vd/F after administration of levodopa/benserazide and levodopa/carbidopa might reflect the higher bioavailability (F) of levodopa with the levodopa/benserazide combination, which was shown in the previous analysis. Intergroup difference of levodopa Vd/F was relatively small between healthy subjects and patients. In contrast, levodopa CL/F was approximately two-thirds lower among the patients than in healthy subjects with both levodopa/DCI formulations. There are many factors that have been reported to affect levodopa pharmacokinetics in PD patients, such as sex, duration of the disease, meal content, time between medication and meal, renal function, and gastric pH.[7–9] Age also seems to have a considerable impact on levodopa pharmacokinetics, because it globally affects organs and functions associated with levodopa absorption, distribution, metabolism and clearance, although reports measuring the impact of age are sparse. In the present study,

Table 1 Levodopa population pharmacokinetics following administration of levodopa/benserazide or levodopa/carbidopa in healthy subjects or patients with Parkinson's disease

	Healthy subjects		Parkinson's disease patients	
	Levodopa/benserazide	Levodopa/carbidopa	Levodopa/benserazide	Levodopa/carbidopa
Population mean				
K_a (1/min)	10 (fixed)	10 (fixed)	10 (fixed)	10 (fixed)
CL/F (L/min)	0.734	0.889	0.493	0.555
Vd/F (L)	44.7	80.0	55.0	81.4
CL/F inter-individual variability (CV%)	12.2	22.4	NE	48.2
CL/F residual variability (CV%)	27.6	32.7	45.8	18.9

CL/F, apparent clearance; CV%, percent coefficient of variation; K_a, absorption rate constant; Vd/F, apparent volume of distribution.

the PD group was older, included women and might have had poorer kidney function compared with the healthy subject group. All those factors would contribute to the lower CL/F in the patient group. Finally, the interindividual variability and residual variability were larger in the PD group, presumably because the study conditions for the patient group were not as rigorously controlled compared with the study in healthy subjects. Nevertheless, the parameters derived from the patient data were similar to those from the healthy subject data.

In clinical settings, both levodopa/DCI combinations have been used for PD patients for decades, and have been generally considered as similarly reliable, although some studies in smaller populations have emphasized differences between DCI. For example, Admani *et al.*[10] reported that levodopa/benserazide showed more improvement in all parkinsonian signs and symptoms compared with levodopa/carbidopa in a double-blind study in 60 PD patients, although the differences did not reach statistically significance. Rinne and Mölsä concluded that levodopa/benserazide 200/50 mg had the same clinically efficacy as levodopa/carbidopa 250/25 mg in a randomized, double-blind, cross-over trial in 49 PD patients, although levodopa/carbidopa induced significantly more nausea and vomiting.[2] Diamond *et al.*[11] carried out a double-blind comparison of levodopa/benserazide and levodopa/carbidopa in 20 PD patients, and reported that the majority of patients fared distinctly better on either levodopa/benserazide or levodopa/carbidopa. In a cross-over study in 19 PD patients, Greenacre *et al.*[12] also found that most patients preferred either levodopa/benserazide or levodopa/carbidopa. These reported differences between levodopa/benserazide and levodopa/carbidopa might be partly explained by our current findings. Levodopa/benserazide would possibly be a better candidate for patients requiring immediate treatment because of its higher C_{max} and stronger DCI efficacy. In contrast, levodopa/carbidopa might be useful for patients with motor complications, such as troublesome dyskinesia, because its levodopa pharmacokinetics is relatively stable.[13–15]

Regarding the dosage of combined carbidopa, not only a tablet of levodopa/carbidopa 100/10 mg, but also a 100/25-mg tablet is available outside Japan. We only used 100/10-mg tablets, so the results of the present study should be carefully translated. A larger proportion of carbidopa is reportedly associated with better therapeutic outcomes and fewer adverse events in some reports, whereas the Japanese approval document concluded that the significant increase of levodopa was not observed with higher carbidopa combinations.[16,17] Although detailed pharmacokinetic features remain unknown, one study showed an approximately 20% increase of levodopa AUC when 450 mg/day carbidopa was orally administered with levodopa infusion, compared with 75 mg/day.[18] The higher carbidopa proportion is possibly associated with a higher C_{max} and AUC, but the impact might be limited. Another limitation of the study is that all the study participants were ethnically identical; that is, they were all Asians. Most previous reports were from the USA and Europe, but there have not been any ethnic factors associated with levodopa pharmacokinetics reported, and the present results are in accord with other reports.

In conclusion, administration of levodopa/benserazide 100/25 mg provided higher levodopa C_{max} and larger $AUC_{0-3\ h}$ as compared with levodopa/carbidopa 100/10 mg. Benserazide had a stronger AADC inhibitory effect, although differences in the pharmacokinetics of systemic benserazide and carbidopa did not seem to contribute to the elimination of levodopa. The population study showed that the pharmacokinetics of levodopa after the administration of levodopa/benserazide and levodopa/carbidopa were similar in PD patients and healthy subjects apart from the lower levodopa CL/F in patients, which could result in the higher AUC of levodopa in patients with Parkinson's disease than healthy volunteers. Levodopa/benserazide might be a better choice for patients with more severe adverse effects or inadequate levodopa efficacy, and levodopa/carbidopa might be more useful for patients with motor complications.

Acknowledgments

The authors thank Masato Fukae and Makoto Katou for their technical support in data analysis. The authors acknowledge a Grant-in-Aid from the Research Committee of Neuromuscular Disorders and Neurodegenerative Disorders, the Ministry of Health, Labor and Welfare of Japan, GJTS, and a Research Grant from Ehime University. The authors declare no conflict of interest.

References

1 Nakatsuka A, Nagai M, Yabe H *et al.* Effect of clarithromycin on the pharmacokinetics of cabergoline in healthy controls and in patients with Parkinson's disease. *J. Pharmacol. Sci.* 2006; **100**: 59–64.
2 Rinne UK, Mölsä P. Levodopa with benserazide or carbidopa in Parkinson disease. *Neurology* 1979; **29**: 1584–9.
3 Korten JJ, Keyser A, Joosten EM *et al.* Madopar versus sinemet. A clinical study on their effectiveness. *Eur. Neurol.* 1975; **13**: 65–71.
4 Stocchi F, Jenner P, Obeso JA. When do levodopa motor fluctuations first appear in Parkinson's disease? *Eur. Neurol.* 2010; **63**: 257–66.
5 Contin M, Riva R, Albani F *et al.* Pharmacokinetic optimisation in the treatment of Parkinson's disease. *Clin. Pharmacokinet.* 1996; **30**: 463–81.
6 Guldberg HC, Marsden CA. Catechol-O-methyl transferase: pharmacological aspects and physiological role. *Pharmacol. Rev.* 1975; **27**: 135–206.
7 Astarloa R, Mena MA, Sánchez V *et al.* Clinical and pharmacokinetic effects of a diet rich in insoluble fiber on Parkinson disease. *Clin. Neuropharmacol.* 1992; **15**: 375–80.
8 Robertson DR, Wood ND, Everest H *et al.* The effect of age on the pharmacokinetics of levodopa administered alone and in the presence of carbidopa. *Br. J. Clin. Pharmacol.* 1989; **28**: 61–9.
9 Doi H, Sakakibara R, Sato M *et al.* Plasma levodopa peak delay and impaired gastric emptying in Parkinson's disease. *J. Neurol. Sci.* 2012; **319**: 86–8.

10 Admani AK, Verma S, Cordingley GJ *et al.* Patient benefits of l-dopa and a decarboxylase inhibitor in the treatment of Parkinson's disease in elderly patients. *Pharmatherapeutica* 1985; **4**: 132–40.
11 Diamond SG, Markham CH, Treciokas LJ. A double-blind comparison of levodopa, Madopa, and Sinemet in Parkinson disease. *Ann. Neurol.* 1978; **3**: 267–72.
12 Greenacre JK, Coxon A, Petrie A *et al.* Comparison of levodopa with carbidopa or benserazide in parkinsonism. *Lancet* 1976; **2**: 381–4.
13 Jenner P. Factors influencing the onset and persistence of dyskinesia in MPTP-treated primates. *Ann. Neurol.* 2000; **47**(Suppl. 1): S90–9.
14 Chaudhuri KR, Rizos A, Sethi KD. Motor and nonmotor complications in Parkinson's disease: an argument for continuous drug delivery? *J. Neural. Transm.* 2013; **120**: 1305–20.
15 Stocchi F. Continuous dopaminergic stimulation and novel formulations of dopamine agonists. *J. Neurol.* 2011; **258**(Suppl. 2): S316–22.
16 Hoehn MM. Increased dosage of carbidopa in patients with Parkinson's disease receiving low doses of levodopa. A pilot study. *Arch. Neurol.* 1980; **37**: 146–9.
17 Tourtellotte WW, Syndulko K, Potvin AR *et al.* Increased ratio of carbidopa to levodopa in treatment of Parkinson's disease. *Arch. Neurol.* 1980; **37**: 723–6.
18 Brod L, Aldred J, Nutt J. Are high doses of carbidopa a concern? A randomized clinical trial in Prakinson's disease. *Mov. Disord.* 2012; **27**: 750–3.

HTLV-1 induces a Th1-like state in CD4+CCR4+ T cells

Natsumi Araya,[1] Tomoo Sato,[1] Hitoshi Ando,[1] Utano Tomaru,[2] Mari Yoshida,[3] Ariella Coler-Reilly,[1] Naoko Yagishita,[1] Junji Yamauchi,[1] Atsuhiko Hasegawa,[4] Mari Kannagi,[4] Yasuhiro Hasegawa,[5] Katsunori Takahashi,[1] Yasuo Kunitomo,[1] Yuetsu Tanaka,[6] Toshihiro Nakajima,[7,8] Kusuki Nishioka,[7] Atae Utsunomiya,[9] Steven Jacobson,[10] and Yoshihisa Yamano[1]

[1]Department of Rare Diseases Research, Institute of Medical Science, St. Marianna University School of Medicine, Kanagawa, Japan. [2]Department of Pathology, Hokkaido University Graduate School of Medicine, Hokkaido, Japan. [3]Institute for Medical Science of Aging, Aichi Medical University, Aichi, Japan. [4]Department of Immunotherapeutics, Tokyo Medical and Dental University, Graduate School, Tokyo, Japan. [5]Department of Neurology, St. Marianna University School of Medicine, Kanagawa, Japan. [6]Department of Immunology, Graduate School of Medicine, University of the Ryukyus, Okinawa, Japan. [7]Institute of Medical Science and [8]Center for Clinical Research, Tokyo Medical University, Tokyo, Japan. [9]Department of Hematology, Imamura Bun-in Hospital, Kagoshima, Japan. [10]Viral Immunology Section, Neuroimmunology Branch, National Institutes of Health, Bethesda, Maryland, USA.

Human T-lymphotropic virus type 1 (HTLV-1) is linked to multiple diseases, including the neuroinflammatory disease HTLV-1–associated myelopathy/tropical spastic paraparesis (HAM/TSP) and adult T cell leukemia/lymphoma. Evidence suggests that HTLV-1, via the viral protein Tax, exploits CD4+ T cell plasticity and induces transcriptional changes in infected T cells that cause suppressive CD4+CD25+CCR4+ Tregs to lose expression of the transcription factor FOXP3 and produce IFN-γ, thus promoting inflammation. We hypothesized that transformation of HTLV-1–infected CCR4+ T cells into Th1-like cells plays a key role in the pathogenesis of HAM/TSP. Here, using patient cells and cell lines, we demonstrated that Tax, in cooperation with specificity protein 1 (Sp1), boosts expression of the Th1 master regulator T box transcription factor (T-bet) and consequently promotes production of IFN-γ. Evaluation of CSF and spinal cord lesions of HAM/TSP patients revealed the presence of abundant CD4+CCR4+ T cells that coexpressed the Th1 marker CXCR3 and produced T-bet and IFN-γ. Finally, treatment of isolated PBMCs and CNS cells from HAM/TSP patients with an antibody that targets CCR4+ T cells and induces cytotoxicity in these cells reduced both viral load and IFN-γ production, which suggests that targeting CCR4+ T cells may be a viable treatment option for HAM/TSP.

Introduction

The flexibility of the CD4+ T cell differentiation program that underlies the success of the adaptive immune response has recently been implicated in the pathogeneses of numerous inflammatory diseases (1–3). The majority of CD4+ T lymphocytes belong to a class of cells known as Th cells, so called because they provide help on the metaphorical immune battlefield by stimulating the other soldiers — namely, B cells and cytotoxic T lymphocytes — via secretion of various cytokines. Interestingly, there is also a minority group of CD4+ T cells with quite the opposite function: Tregs actively block immune responses by suppressing the activities of CD4+ Th cells as well as many other leukocytes (4). Tregs are credited with maintaining immune tolerance and preventing inflammatory diseases that could otherwise occur as a result of uninhibited immune reactions (5). Thus, the up- or downregulation of certain CD4+ T cell lineages could disrupt the carefully balanced immune system, threatening bodily homeostasis.

The plasticity of CD4+ T cells, particularly Tregs, makes CD4+ T cell lineages less clean-cut than they may originally appear. CD4+ T cells are subdivided according to various lineage-specific chemokine receptors and transcription factors they express, as well as the cytokines they produce (6). Th1 cells, for example, can be identified by expression of CXC motif receptor 3 (CXCR3) and T box transcription factor (T-bet; encoded by *TBX21*) and are known to secrete the proinflammatory cytokine IFN-γ (6). While both have been known to express CC chemokine receptor 4 (CCR4) and CD25, Th2 cells and Tregs can usually be distinguished from each other by their expression of GATA-binding protein 3 (GATA3) and forkhead box p3 (FOXP3), respectively (6, 7). CCR4 is coexpressed in the majority of CD4+FOXP3+ cells and in virtually all CD4+CD25+FOXP3+ cells, making it a useful — albeit not fully specific — marker for Tregs (8, 9). FOXP3 is a particularly noteworthy marker because its expression is said to be required for Treg identity and function (10). In fact, *Foxp3* point mutations are reported to cause fatal multiorgan autoimmune diseases (11). Even partial loss of FOXP3 expression can disrupt the suppressive nature of Tregs, representing one of several pathways by which even fully differentiated Tregs can reprogram into inflammatory cells (12). There have been several reports of Tregs reprogramming in response to proinflammatory cytokines such as IL-1, IL-6, IL-12, and IFN-γ (12, 13); it is thought that this reprogramming may have evolved as an adaptive mechanism for dampening immune suppression when protective inflammation is necessary (12). However, this same plasticity can lead to pathologically chronic inflammation, and several autoimmune diseases have been associated with reduced FOXP3 expression and/or Treg function, including multiple sclerosis, myasthenia gravis, and type 1 diabetes (14, 15).

Of the roughly 10–20 million people worldwide infected with human T-lymphotropic virus type 1 (HTLV-1), up to 2%–3% are affected by the neurodegenerative chronic inflammatory dis-

Conflict of interest: The authors have declared that no conflict of interest exists.
Submitted: January 17, 2014; **Accepted:** May 8, 2014.
Reference information: *J Clin Invest.* 2014;124(8):3431–3442. doi:10.1172/JCI75250.

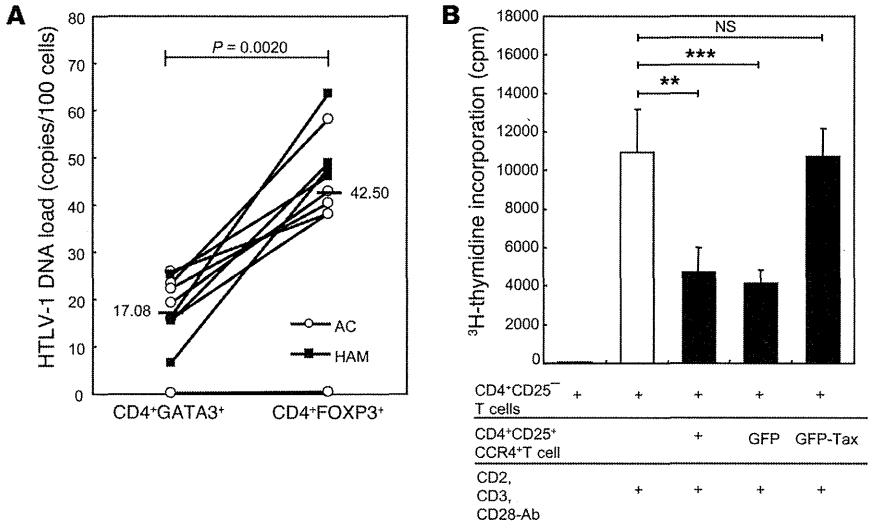

Figure 1. HTLV-1 mainly infects Tregs and inhibits their regulatory function. (**A**) Higher HTLV-1 proviral DNA load in CD4⁺FOXP3⁺ cells (Tregs) compared with CD4⁺GATA3⁺ cells ($P = 0.0020$, Wilcoxon test) from asymptomatic carriers (AC; $n = 6$) and HAM/TSP patients ($n = 4$). PBMCs were FACS sorted, and proviral load was measured using quantitative PCR. Horizontal bars represent the mean value for each set. (**B**) Loss of regulatory function in Tax-expressing CD4⁺CD25⁺CCR4⁺ cells (Tregs). CD4⁺CD25⁻ T cells from an HD were stimulated with CD2, CD3, and CD28 antibodies and cultured alone or in the presence of equal numbers of CD4⁺CD25⁺CCR4⁺ T cells, GFP lentivirus–infected HD CD4⁺CD25⁺CCR4⁺ T cells, or GFP-Tax lentivirus–infected HD CD4⁺CD25⁺CCR4⁺ T cells. As a control, CD4⁺CD25⁻ T cells alone were cultured without any stimulus. Proliferation of T cells was determined using ^{3}H-thymidine incorporation by adding ^{3}H-thymidine for 16 hours after 4 days of culture. All tests were performed in triplicate. Data are mean ± SD. $^{**}P < 0.01$, $^{***}P < 0.001$, ANOVA followed by Tukey test for multiple comparisons.

ease HTLV-1–associated myelopathy/tropical spastic paraparesis (HAM/TSP). The main other condition associated with the retrovirus is adult T cell leukemia/lymphoma (ATLL), a rare and aggressive cancer of the T cells. HAM/TSP represents a useful starting point from which to investigate the origins of chronic inflammation, because the primary cause of the disease — viral infection — is so unusually well defined. HAM/TSP patients share many immunological characteristics with FOXP3 mutant mice, including multiorgan lymphocytic infiltrates, overproduction of inflammatory cytokines, and spontaneous lymphoproliferation of cultured CD4⁺ T cells (16–18). We and others have proposed that HTLV-1 preferentially infects CD4⁺CD25⁺CCR4⁺ T cells, a group that includes Tregs (7, 19). Samples of CD4⁺CD25⁺CCR4⁺ T cells isolated from HAM/TSP patients exhibited low FOXP3 expression as well as reduced production of suppressive cytokines and low overall suppressive ability — in fact, these CD4⁺CD25⁺CCR4⁺FOXP3⁻ T cells were shown to produce IFN-γ and express Ki67, a marker of cell proliferation (19). The frequency of these IFN-γ–producing CD4⁺CD25⁺CCR4⁺ T cells in HAM/TSP patients was correlated with disease severity (19). Finally, evidence suggests that the HTLV-1 protein product Tax may play a role in this alleged transformation of Tregs into proinflammatory cells in HAM/TSP patients: transfecting Tax into CD4⁺CD25⁺ cells from healthy donors (HDs) reduced FOXP3 mRNA expression, and Tax expression in CD4⁺CD25⁺CCR4⁺ cells was higher in HAM/TSP versus ATLL patients despite similar proviral loads (19, 20). Therefore, we hypothesized that HTLV-1 causes chronic inflammation by infecting CD4⁺CD25⁺CCR4⁺ T cells and inducing their transformation into Th1-like, IFN-γ–producing proinflammatory cells via intracellular Tax expression and subsequent transcriptional alterations including but not limited to loss of endogenous FOXP3 expression.

In this study, we first sought to discover the detailed mechanism by which Tax influences the function of CD4⁺CD25⁺CCR4⁺ T cells. We used DNA microarray analysis of CD4⁺CD25⁺CCR4⁺ T cells from HAM/TSP patients to identify *TBX21*, known as a master transcription factor for Th1 differentiation, as a key intermediary between Tax expression and IFN-γ production. We demonstrated that Tax, in concert with specificity protein 1 (Sp1), amplified *TBX21* transcription and subsequently IFN-γ production. Next, we established the presence of Th1-like CD4⁺CCR4⁺ T cells in the CSF and spinal cord lesions of HAM/TSP patients. The majority of these CD4⁺CCR4⁺ T cells coexpressed CXCR3 as well as T-bet and IFN-γ. Finally, we investigated the therapeutic potential of an anti-CCR4 monoclonal antibody with antibody-dependent cellular cytotoxicity (ADCC) (21). Applying this antibody in vitro diminished the proliferative capacity of cultured PBMCs and reduced both proviral DNA load and IFN-γ production in cultured CSF cells as well as PBMCs. In conclusion, we were able to elucidate a more detailed mechanism for the pathogenesis of HAM/TSP and use our findings to suggest a possible therapeutic strategy.

Results

HTLV-1 preferentially infects Tregs and alters their behavior via Tax. Experiments were conducted to determine which among CD4⁺CD25⁺CCR4⁺ T cells were infected by HTLV-1, and how the infection influenced their functionality. Analysis of fluorescence-activated cell sorting (FACS)-sorted PBMCs obtained from asymptomatic carriers ($n = 6$) as well as HAM/TSP patients ($n = 4$) revealed that Tregs (CD4⁺FOXP3⁺) carried much higher proviral loads than Th2 cells (CD4⁺GATA3⁺) ($P = 0.0020$; Figure 1A). As it is well established that each infected cell contains only 1 copy of the HTLV-1 provirus (22, 23), these results indicate that a larger proportion of FOXP3⁺ than GATA3⁺ CD4⁺ T cells are infected. As expected, proliferation of CD4⁺CD25⁻ cells after stimulation, as measured by ^{3}H-thymidine incorporation, was suppressed upon coculture with CD4⁺CD25⁺CCR4⁺ cells, including Tregs ($n = 3$, $P < 0.01$; Figure 1B). However, after being transduced with lentiviral vector expressing GFP-Tax, the CD4⁺CD25⁺CCR4⁺ cells no longer suppressed cell proliferation; conversely, cells transduced with the control vector expressing only GFP retained full suppressive function ($P < 0.001$; Figure 1B).

The HTLV-1 protein product Tax induces IFN-γ production via T-bet. Experiments were conducted to determine if and how Tax affects IFN-γ production in infected T cells. First, the existence of a functional link between *Tax* and *IFNG* was established by using the